Diploma thesis

Surface characterization of cellulose fibers by atomic force microscopy in liquid media and under ambient conditions

by
Christian Ganser

at the Institute of Physics
Montanuniversität Leoben, Austria

under supervision of
Ao. Univ. Prof. Dr. Christian Teichert
Dipl.-Ing. Dr.mont. Franz J. Schmied

refereed by
Ao. Univ. Prof. Dr. Christian Teichert

Leoben, June 2011

dedicated to my parents

Eidesstattliche Erklärung

Ich erkläre an Eides statt, dass ich diese Arbeit selbständig verfasst, andere als die angegebenen Quellen und Hilfsmittel nicht benutzt und mich auch sonst keiner unerlaubten Hilfsmittel bedient habe.

Affidavit

I declare in lieu of oath, that I wrote this thesis and performed the associated research myself, using only literature cited in this volume.

Christian Ganser
Leoben, June 2011

Abstract

Nowadays, cellulose fibers are widely used for paper, textile, and hygiene products. While paper is produced using native cellulose fibers extracted from wood, cellulose fibers for textiles and hygiene products are manufactured from regenerated cellulose fibers. Native cellulose fibers are called cellulose type I fibers, whereas regenerated cellulose fibers are called cellulose type II fibers. The raw material for both fiber types is wood. Native cellulose fibers are wood cells which are composed of cellulose, hemicelluloses and lignin and are extracted from the wood matrix by the pulping process. Regenerated cellulose fibers are produced by dissolving the cellulose from pulp and spinning it into fibers.

The native cellulose fibers investigated in this work were spruce and pine kraft pulp fibers, provided by an industrial supplier. The pulp fibers were treated at different temperatures, which led to a decrease in mechanical properties of a formed sheet. The fiber surfaces were characterized by atomic force microscopy (AFM) in wet and dry state. Dried pulp fibers show a wrinkled surface. Pulp fibers in wet state – measured in an aqueous environment – reveal a smoother surface with only a few wrinkles. Also single microfibrils with a diameter of about 120 nm and lignin precipitates could be observed in AFM topography images. On spruce pulp fibers, the investigated surface layer was identified as the secondary wall number one, whereas on pine pulp fibers the primary wall was found to be the exposed layer. Additionally, pine pulp fiber surfaces showed a higher coverage of lignin precipitates than spruce pulp fiber surfaces.

The investigated regenerated cellulose fibers were viscose type fibers directly taken from the production line. Classical viscose fibers with a cloud-shaped cross-section and fibers with a collapsed, hollow cross-section were characterized. One of the hollow viscose fiber samples was modified by carboxymethyl cellulose (CMC). This modification increased the negative surface charge. On the hollow fibers, surface wrinkles in the range of 500 nm to 1000 nm were observed. The classical viscose fibers showed surface wrinkles with a size of about 3000 nm. Also, the fibrillar fine structure was visualized using AFM phase imaging in tapping mode where a fibril width between 30 nm and 40 nm was obtained. The amount of CMC – determined by AFM – on the scanned region of the modified sample was three times the added amount.

Kurzfassung

Heutzutage werden Cellulosefasern für Papier-, Textil-, und Hygieneprodukte benutzt. Während Papier aus natürlichen Cellulosefasern, extrahiert aus Holz, produziert wird, werden Textilien und Hygieneprodukte aus regenerierten Cellulosefasern hergestellt. Natürliche Cellulosefasern sind Cellulosefasern vom Typ I, wohingegen regenerierte Fasern Cellulosefasern vom Typ II sind. Das Rohmaterial für beide Fasertypen ist Holz. Natürliche Cellulosefasern sind Holzzellen, welche aus Cellulose, Hemicellulosen und Lignin bestehen und durch den Prozess des Aufschlusses aus der Holzmatrix extrahiert werden. Regenerierte Cellulosefasern werden durch Lösen der Cellulose aus Zellstoff und anschließendem Faserspinnen hergestellt.

Die in dieser Arbeit untersuchten natürlichen Cellulosefasern waren Kraftzellstofffasern von Fichten und Kiefern, welche von einem Industriepartner zur Verfügung gestellt wurden. Die Zellstofffasern wurden bei verschiedenen Temperaturen behandelt, was zu einem Verlust an mechanischen Eigenschaften eines daraus geformten Blattes führte. Die Faseroberflächen wurden durch Rasterkraftmikroskopie (AFM) in nassem und trockenem Zustand untersucht. Getrocknete Zellstofffasern zeigen eine faltige Oberfläche. Zellstofffasern in nassem Zustand – gemessen in einer wässrigen Umgebung – zeigen eine glatte Oberfläche mit nur wenigen Falten. Es konnten auch einzelne Mikrofibrillen mit einem Durchmesser von etwa 120 nm und Ligninprezipitate in AFM Topographiebildern beobachtet werden. Bei Zellstofffasern von Fichten war die untersuchte Oberflächenschicht die Sekundärwand Nummer eins, wohingegen bei Zellstofffasern von Kiefern die Primärwand die freigelegte Schicht war. Zusätzlich zeigten Zellstofffasern von Kiefern eine höhere Bedeckung von Ligninprezipitaten als Zellstofffaseroberflächen von Fichten.

Die untersuchten regenerierten Cellulosefasern waren direkt aus der Produktionslinie entnommene Viskosefasern. Klassische Viskosefasern mit einem wolkenartigen Querschnitt und Fasern mit einem hohlen, kollabierten Querschnitt wurden charakterisiert. Eine der hohlen Viskosefaserproben wurde durch Carboxymethyl Cellulose (CMC) modifiziert. Diese Modifikation erhöhte die negative Oberflächenladung. Bei den hohlen Fasern wurden Oberflächenfalten im Bereich von 500 nm bis 1000 nm beobachtet. Die klassischen Viskosefasern zeigen Falten von etwa 3000 nm. Es konnte auch die fibrilläre Feinstruktur durch AFM Phasenabbildung im sogenannten Tapping Mode sichtbar gemacht werden wobei eine Fibrillenweite zwischen 30 nm und 40 nm ermittelt wurde. Die Menge an CMC – bestimmt durch AFM – auf der abgerasterten Region der modifizierten Probe war das Dreifache der hinzugegebenen Menge.

Acronyms

σ	Root mean square (RMS) roughness
1D	One-dimensional
2D	Two-dimensional
AFM	Atomic Force Microscopy
CMC	Carboxymethyl cellulose
DP	Degree of polymerization
FFT	Fast Fourier transform
FT	Fourier transform
HHCF	Height-height correlation function
KPFM	Kelvin Probe Force Microscopy
L	Lumen
MFA	Microfibrillar angle
ML	Middle lamella
OM	Optical Microscopy
P	Primary wall
pDADMAC	Polydiallyldimethylammoniumchlorid
PSD	Power spectral density
S1	Secondary wall number one
S2	Secondary wall number two
S3	Secondary wall number three
SEM	Scanning Electron Microscopy

Contents

1 Motivation

Paper is a material used for over 2000 years by mankind [1]. It is utilized as a data storage medium, for packaging, hygiene products, and more. Today it is one of the oldest storage mediums still in use and it will be so probably for many years to come. Even after the extensive use of this material, the bonding mechanisms between its constituents, the indicated cellulose fibers, are not yet fully understood, making it an interesting topic of research.

To investigate the bonding mechanisms in paper, the Christian Doppler Laboratory for *Surface Chemical and Physical Fundamentals of Paper Strength* was established in 2007. It is a collaboration between three university institutes, the Institute of Solid State Physics (Graz University of Technology), the Institute for Paper-, Pulp-, and Fibre Technology (Graz University of Technology) and the Institute of Physics (Montanuniversität Leoben). Beside these university institutes, the industrial partners Mondi, Kelheim Fibres GmbH, and Lenzing AG are incorporated. The investigations at the Institute of Physics (Montanuniversität Leoben) are carried out in the SPM Group using Atomic Force Microscopy (AFM) and AFM-based methods to characterize surface properties.

The first of the two main topics of this work was the investigation of never dried pulp fiber surfaces in water. The reason for these measurements were a significant loss in tensile strength of formed sheets, a reduction of the lignin content and an increased fiber curl. To find an explanation for the loss in tensile strength, the fiber surface morphology is considered to be one possible influencing parameter. The difficulty is that the pulp fibers should not dry before or during the measurements, because the fiber-fiber bonds are formed when the fibers are still wet and drying would lead to a change in morphology and to the occurrence of hornification. Therefore, it was decided to measure the fibers in an aqueous environment, since AFM as tool of choice is known for a long time to allow measurements in liquid environments [2]. Up to now there have been some attempts to measure pulp fibers in water using AFM and the results showed that it is possible, but not an easy task [3,4].

The second topic of this thesis is dedicated to regenerated cellulose fibers, especially viscose fibers. Viscose fibers are man-made cellulose fibers and are made from pulp with certain requirements concerning cellulose, hemicellulose, and lignin contents [5]. Because they are artificially produced, they provide relatively well defined surfaces which can be used as a model system for characterizing fiber-fiber bonds with regard to the surface morphological influence. These fibers can also be added to pulp, leading to a change in properties of the produced paper [6]. It is also known that additives can influence the bonding mechanisms of regenerated (and native) cellulose fibers [7]. One of this additives is carboxymethyl cellulose (CMC), which was used to modify

fibers investigated in this work. The question here was, if it is possible to visualize the attached CMC on the fiber surface by AFM and to quantify the amount of CMC on the surface as well as its distribution on the fiber surface.

2 Theoretical Background

2.1 General constituents of cellulose fibers

Cellulose fibers consist primarily of cellulose, hemicelluloses, and lignin [8]. Regenerated cellulose fibers – in particular – are only made of cellulose whereas native fibers consist of all three constituents. Cellulose is a polymer of D-glucose basic units with cellobiose as the repeating building block, as shown in figure 2.1. The degree of polymerization (DP), however, is actually the number n of repeating anhydroglucose units and reaches from 9,000 up to 15,000 [8,9].

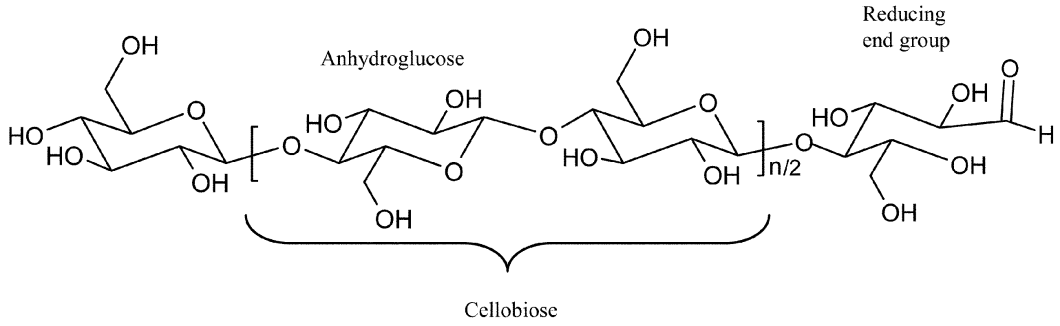

Figure 2.1: The structure of a cellulose macromolecule. Anhydroglucose is the basic unit and cellobiose the repeating unit, n is the DP. (From [9].)

Hemicelluloses are polymers consisting of different sugar monomers like D-xylose, D-glucose, D-galactose, L-arabinose, etc.. They have a lower DP than cellulose (100–200) and are branched. Lignins are different from cellulose and hemicellulose as they are complex, three-dimensional polymers of phenylpropane units. While hemicellulose and lignin are solely amorphous, cellulose has crystalline (up to 65%) and amorphous regions [8].

2.2 Native cellulose fibers

Native cellulose fibers for papermaking are mainly extracted from softwood. Here, the focus was put on pine and spruce fibers which are mainly used as raw material by the industrial collaboration partner Mondi [10]. As already mentioned, native fibers consist of all three main components, where cellulose is mainly found in the microfibrils. Hemicellulose and lignin are composing the matrix which glues and stiffens the natural compound [11].

Wood itself has a hierarchical structure and as the pulp fibers used to be the tracheids (wood cells) in the living plant, they are also hierarchically composed. The lowest level of hierarchy is the D-glucose monomer, followed by the cellulose macromolecule (see section 2.1). These polymer chains form the elementary fibrils, which build up the microfibrils. The microfibrils, together with hemicellulose and lignin, form the cell walls and further the whole cell. To end up with wood, many cells are linked together. Figure 2.2 presents a sketch of the described hierarchical structure of wood.

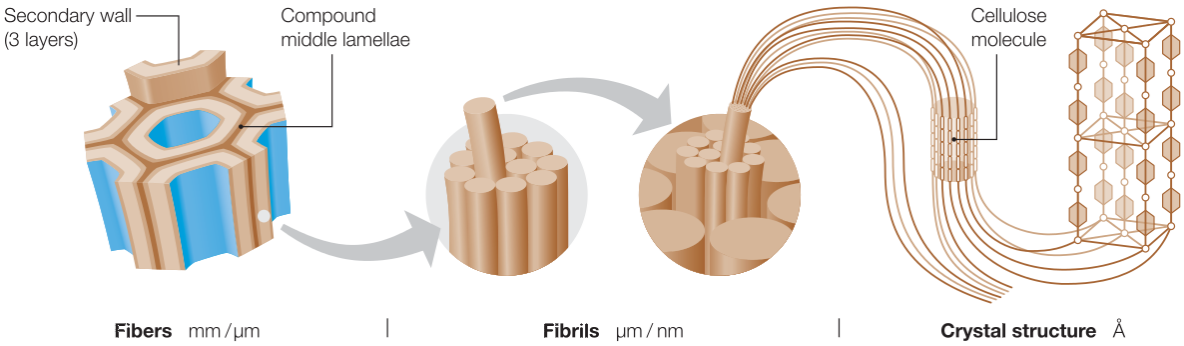

Figure 2.2: The hierarchical structure of wood, from a cellulose chain to the final fiber (cell). (From [12].)

The wood fibers themself are long and slender, have a rectangular cross section with a hollow center, and consist of several cell walls. The fiber geometry varies between the individual wood species, but for spruce and pine the fibers are typically about 2–3 mm long and 14–46 μm wide [13,14]. As presented in figure 2.3a, fibers are made up of different layers, the so called cell walls. The first wall is the primary wall (P), which consists of randomly oriented microfibrils and high amounts of lignin. Adjacent to the inner side of the P wall is the secondary wall number one (S1), followed by the secondary wall number two (S2) and the secondary wall number three (S3). All three secondary layers exhibit an orientation of the microfibrils and the lignin content is decreasing from S1 to S3, where S3 contains almost no lignin. The S2 layer is the thickest and therefore responsible for the major mechanical and physical properties. At the outside, the P layer borders the middle lamella (ML), which glues the individual cells together [8,14]. The hollow part in the center of the fiber is called the lumen where in a living tree the water and nutrients are transported.

The mentioned orientation of the cell walls is characterized by the microfibrillar angle (MFA). The MFA is the angle between the cellulose microfibrils and the long axis of the fiber. In the S1 and S3 walls the MFA has large values, i.e., the fibrils wind around the fiber with a low slope, whereas the MFA in the S2 wall is small, which means a steeper slope [14,15]. The sign of the MFA characterizes the type of the helix in which the microfibrils wind around the fiber. The MFA can always be expressed by an angle in the range of $-90° < \text{MFA} < 90°$, where a positive MFA is presented in figure 2.3b and a negative MFA in figure 2.3c. A positive MFA describes the microfibrils winding around the fiber in a left-handed helix whereas a negative MFA describes a right-handed helix.

The microfibrils in the S1 layer as well as in the S3 layer can change their arrangement from a left-handed to a right-handed helix, but the microfibrils in the S2 layer are always oriented in a right-handed helix [15].

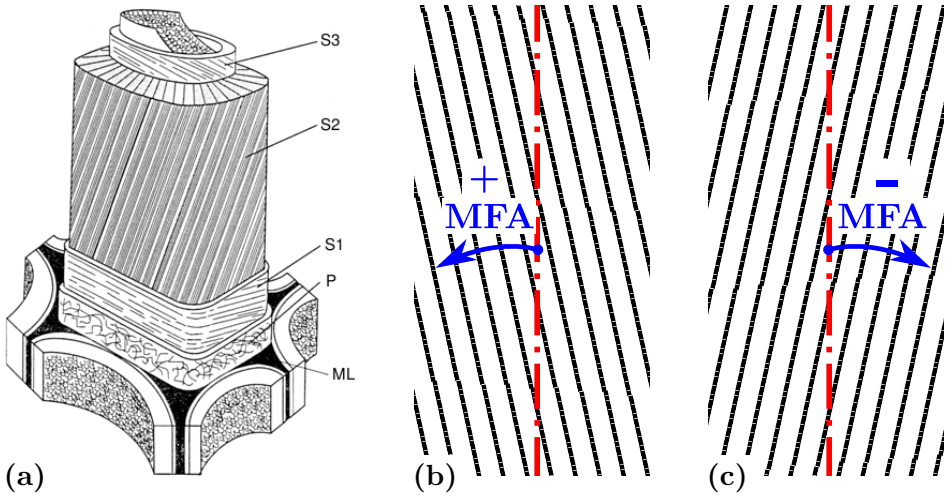

Figure 2.3: (a) Schematic of a wood fiber. (From [11].) (b) Positive MFA (left-handed helix). (c) Negative MFA (right-handed helix). ML–middle lamella, P–primary wall, S1–secondary wall number one, S2–secondary wall number two, S3–secondary wall number three.

The extraction of cellulose fibers from wood can be done mechanically or chemically. The method used worldwide most is chemical pulping, and of all chemical pulping processes, the so called kraft pulping process is employed most. Kraft pulping is a chemical process, where the cellulose fibers are extracted from the matrix by cooking wood chips in a solution of sodium hydroxide and sodium sulfide. In this process, the lignin in the matrix is degenerated and thereby dissolved. It is, however, not possible to dissolve the whole lignin, which leads to a certain residual amount of lignin, dependent on cooking temperature, cooking time, and concentration of the cooking chemicals. To measure the amount of lignin the so called kappa number is introduced, where a low kappa number means a low lignin content and a high kappa number corresponds to a high lignin content. The dissolution is, of course, not only limited to lignin, also hemicelluloses and cellulose are dissolved, limiting the amount of lignin that can be removed. The word "kraft" originates from the Swedish (and German) word for "strength", indicating the superior mechanical properties of papers made by this process [16,17].

2.3 Regenerated cellulose fibers

As already mentioned, cellulose is the main constituent of regenerated fibers. It is, however, a different type of cellulose than in native fibers, the so called cellulose type II. Cellulose found in native fibers is called cellulose type I and forms into cellulose type II

when treated with sodium hydroxide or after dissolution and regeneration [18]. Figure 2.4 shows the difference of cellulose type I and type II in the molecular structure. Cellulose type II is thermodynamically more stable than cellulose type I [19].

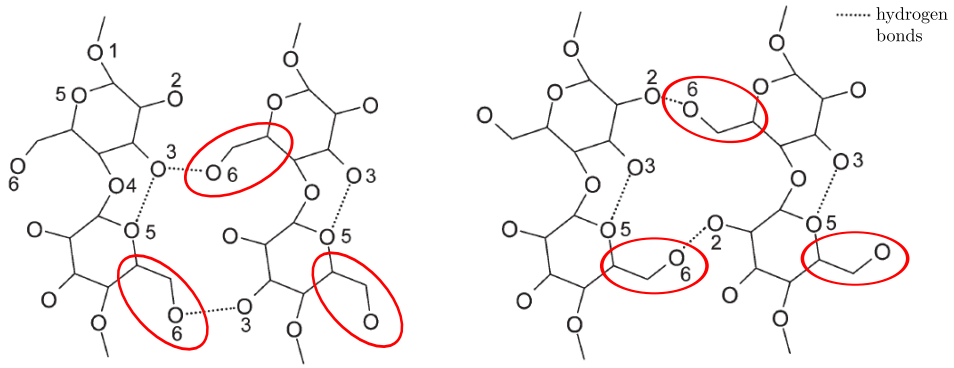

(a) **(b)**

Figure 2.4: The difference (marked with red ellipses) between (a) cellulose type I and (b) cellulose type II. (From [9].)

To manufacture viscose type regenerated fibers, pulp is treated as a first step with sodium hydroxide. This process is called mercerization and produces the swollen Na-cellulose. With addition of carbon disulfide, Na-cellulose reacts to cellulose xanthate, which is dissolved in sulfuric acid. The dissolution in sulfuric acid is called regeneration and leads to a viscose liquid of cellulose type II in solution (hence the name "viscose fibers"). The regenerated cellulose is spun to fibers from a spinning bath using spinnerets (spinning nozzles), which shape the cross-sections of the fibers. There are many different cross-sections possible, also hollow cross-sections, and each has its own applications, which are, for example, hygiene products, textiles and filters [20]. Figure 2.5 shows the difference of the fiber shape between classical and Bellini viscose fibers, which were only investigated in this work. Classical viscose fibers have typically a cloud shaped cross-section, as shown in figure 2.5a. Bellini fibers are in contrast hollow and collapsed. Therefore, they appear flat (see figure 2.5b).

To modify bonding strength of fibers, it is possible to add chemical linkers like starch, polydiallyldimethylammoniumchlorid (pDADMAC), CMC and so on. While CMC modifies the fiber surface to be anionic, starch and pDADMAC are cationic [23–25]. CMC, mostly in the form of NaCMC, is a water soluble cellulose ether and formed by the reaction of cellulose with sodium hydroxide and chloroacetic acid [18,26]. Its molecular structure is presented in figure 2.6.

Furthermore, CMC is used in petroleum, paints, printing, pharmaceutical and foodstuff industries [27]. In food industries CMC is referred to as E 466 and is used as a food additive for fruit preparations, sweets, nuts, etc. [28]. A scientific application of CMC is to use it in an aqueous solution for purification and dispersion of single-wall carbon nanotubes [29].

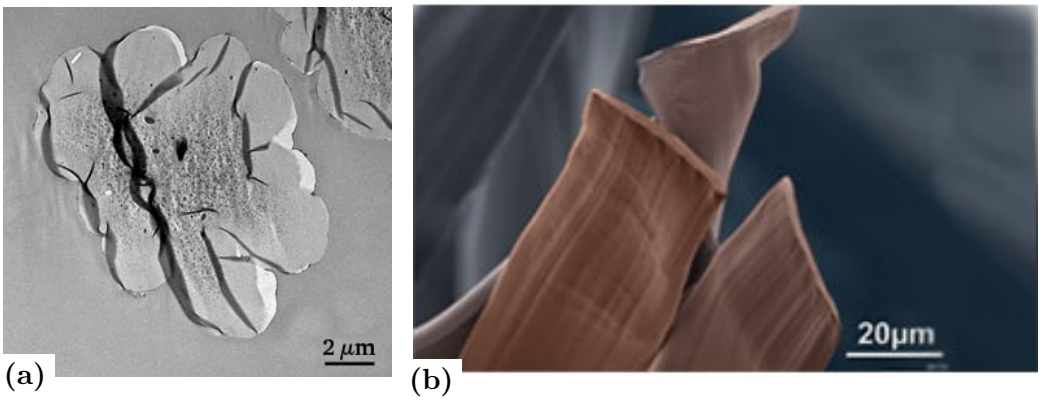

(a) (b)

Figure 2.5: A transmission electron microscopy (TEM) cross section of a (a) classical viscose fiber (from [21]) and a scanning electron microscopy (SEM) image of (b) Bellini fibers. (From [22].)

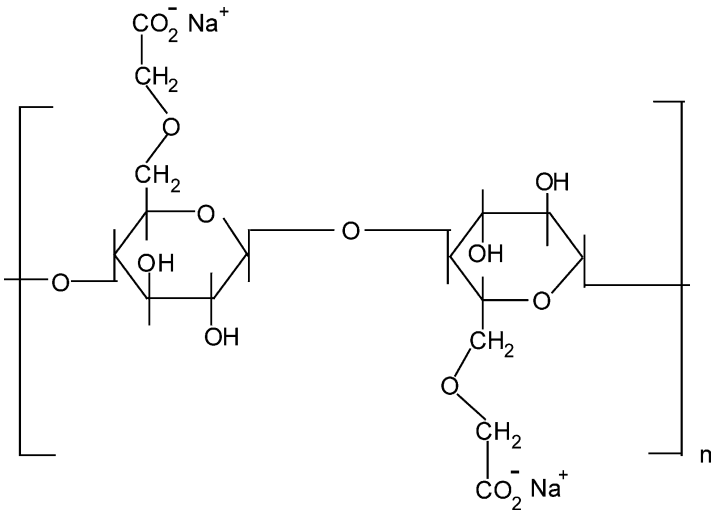

Figure 2.6: The molecular structure of NaCMC. (From [26].)

2.4 Atomic Force Microscopy

2.4.1 Measurement principle

All investigations in this work were carried out using the modern method atomic force microscopy which will be described in the following section. The basic principle of AFM is the scanning of a sharp tip at the end of a cantilever across a surface. The deflection of the cantilever is used to record the height information from the sample surface [30]. The movement of the tip relative to the surface, in lateral directions (x-y-plane) as well as in the direction perpendicular to it (z-direction), is realized using piezoelectric actuators. For detection of the cantilever deflection, the most commonly used method is the laser beam deflection method. Here, a laser illuminates the reflective

coated backside of the cantilever and is reflected to a split photodiode. A change of the cantilever deflection moves the laser spot on the split photodiode. This movement can be measured by the difference of the signals between the upper and lower half of the photodiode, which is proportional to the cantilever deflection. Figure 2.7 represents a scheme of AFM.

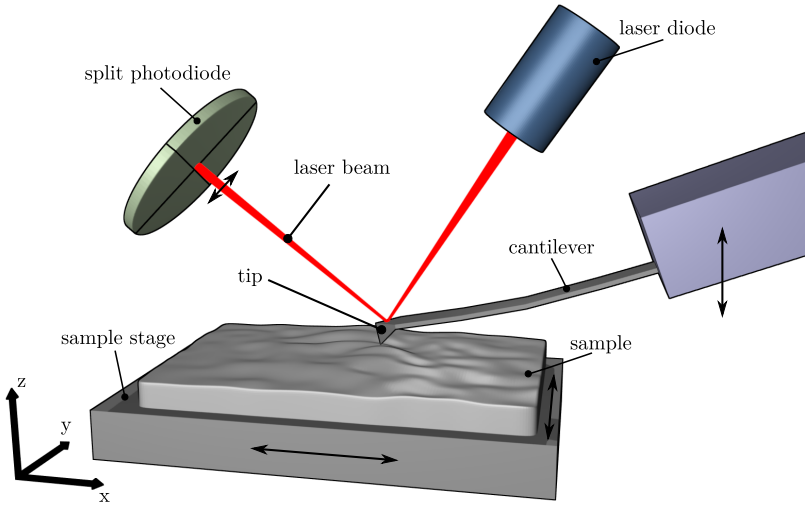

Figure 2.7: Schematic principle of AFM, employing laser deflection as read out method of the cantilever deflection. The arrows indicate the possible movement of the piezoelectric actuators, which are not drawn explicitly.

There are in principle three AFM measurement modes: contact mode, non-contact mode and tapping mode. In contact mode, the tip stays permanently in contact with the sample surface and the cantilever deflection is used as the signal to get height information by either keeping the deflection constant and recording the z-piezo movement or keeping the height constant and recording the deflection.

In non-contact mode, the cantilever is oscillating near its resonance frequency at a distance from the surface, not touching it. If the distance between tip and surface decreases, the amplitude is more damped. This can be detected and used to adjust the height by movement of the z-piezo, which is then proportional to the surface topography. Using so called qPlus sensors, this technique is able to image smooth surfaces with atomic resolution [31].

Tapping mode is now a combination of contact and non-contact mode. The cantilever is again oscillating near its resonance frequency but periodically tapping the surface [32]. This also allows high resolution imaging and reduces sample damage. Thus, tapping mode is a good choice for imaging biological materials, which are usually soft materials. The height information is obtained in the same way as in non-contact mode. Additionally, in tapping mode also the phase shift between the exciting oscillation and the actual oscillation of the cantilever can be recorded and stored as a so called phase image. The lag between the two oscillations is proportional to the dissipated energy [33].

AFM in tapping mode has also been proved to be a reliable method to measure samples in liquids, such as water [2]. In this case, a shift of the resonance frequency to lower values, as well as a broadening of the resonance peak due to the increased damping is observed. Thus, it is more difficult to establish stable measurement conditions.

To enhance the resonance curve of the cantilever in air and in liquids, a so called Q-control can be used to actively increase the Q-factor, which is defined as

$$Q = \frac{f_{res}}{\Delta f}. \tag{2.1}$$

In equation 2.1, Δf and f_{res} denote the width of the resonance curve and the resonance frequency respectively [34]. Q-control is achieved by adding a feedback circuit to the cantilevers oscillation with a phase shift ϕ and an adjustable Q-gain G, so that the equation of motion of the oscillating cantilever reads

$$m\ddot{z}(t) - \alpha\dot{z}(t) - kz(t) = F_0\cos(\omega t) + Ge^{i\phi}z(t), \tag{2.2}$$

where α denotes the damping constant, m the effective cantilever/tip mass, k the cantilevers spring constant, F_0 the oscillation magnitude, and ω the oscillation frequency [34]. By assuming a sinusoidal cantilever motion $z(t)$ and a phase shift of $\pm\frac{\pi}{2}$, equation 2.2 simplifies to

$$m\ddot{z}(t) - \alpha_{eff}\dot{z}(t) - kz(t) = F_0\cos(\omega t), \tag{2.3}$$

with $\alpha_{eff} = \alpha + G$. This means that with Q-control, it is possible to adjust the effective damping constant and by that the effective Q-factor Q_{eff}, which is inversely proportional to the effective damping constant [34].

2.4.2 Methods for analysis of AFM images

The free software Gwyddion was used to analyze the obtained experimental data [35]. It allows the visualization of the acquired AFM data and includes extensive data processing utilities. Several functions for data evaluation are also implemented, like fast fourier transform (FFT), the power spectral density (PSD), and the height-height correlation function (HHCF), which were used for characterizing the fiber surfaces. These methods proved to be useful already in preceding works on characterization of fiber surfaces [36,37].

The fourier transform (FT) is implemented by the FFT algorithm [38] utilizing the FFTW3 library [39] and gives information about the harmonic components of an image. A condition for the FFT algorithm to work is that the number of transformable data points is of the form 2^n. Therefore, all AFM images presented here are recorded in a 512×512 pixel matrix, but it would also be possible to apply the FFT algorithm to images with a size of, for example, 512×2048 pixels. FFT analysis reveals the preferred feature arrangement and thus allows the determination of fibril orientation.

The 2D HHCF $C(\mathbf{r})$ is in general given by

$$C(\mathbf{r}) = \langle [z(\mathbf{r}_0 + \mathbf{r}) - \langle z \rangle][z(\mathbf{r}_0) - \langle z \rangle] \rangle, \tag{2.4}$$

where $\mathbf{r}$ is the 2D vector (x_i, y_j) of a point on the surface and $z = z(x_i, y_j)$ is its height [40]. For a discrete height map, the HHCF can be written as

$$C(m,n) = \frac{1}{(N-n)(M-m)} \sum_{k=1}^{N-n} \sum_{l=1}^{M-m} z_{k+m,l+n} z_{k,l}, \tag{2.5}$$

with $m = \frac{x_1 - x_2}{\Delta x}$ and $n = \frac{y_1 - y_2}{\Delta y}$, where (x_1, y_1) and (x_2, y_2) are two data points and Δx and Δy are the sampling intervals of the AFM image in x- and y-direction respectively. In Gwyddion the calculation of the HHCF is implemented as the HHCF of a single scan line and averaged over all horizontal lines, which reduces equation 2.5 to

$$C_x(m) = C(m,0) = \frac{1}{N(M-m)} \sum_{k=1}^{N-n} \sum_{l=1}^{M-m} z_{k+m,l} z_{k,l}. \tag{2.6}$$

Equation 2.6 is called the one-dimensional (1D) HHCF [41]. By fitting the HHCF with the function

$$C(\mathbf{r}) = \sigma^2 e^{-\left(\frac{|\mathbf{r}|}{\xi}\right)^{2\alpha}}, \tag{2.7}$$

a self-affine random rough surface with a cutoff in roughness increase can be characterized by the parameters σ, ξ, α. Here, σ denotes the root mean square roughness of the surface, which can be calculated by

$$\sigma = \sqrt{\frac{1}{N^2} \sum_{i=1}^{N} \sum_{j=1}^{N} [z(x_i, y_j) - \langle z \rangle]^2}. \tag{2.8}$$

ξ is called the lateral correlation length, this is the distance between two points, for that their heights are still correlated. The last parameter α, the roughness exponent or Hurst parameter, describes the jaggedness of the surface ($\alpha = 0.5 \ldots$ more jagged, $\alpha = 1 \ldots$ less jagged) [40,42]. The applied fit of the experimental data to equation 2.7 to calculate the roughness parameters was performed with the non-linear Levenberg-Marquardt algorithm [43,44].

The PSD is the FT of the HHCF and allows the determination of feature sizes such as average microfibril diameter and average size of surface wrinkles. Figure 2.8 shows the 1D PSD of figure 2.9a taken at the angle α. The feature sizes are calculated by fitting a Gaussian function to a peak and taking the reciprocal of the peak position. The width of the peak at half maximum gives the variance of the feature sizes. The first peak in figure 2.8 corresponds to the black lines in figure 2.9a, the second and third peaks are its higher orders. The highest peak at $2.5\,\mu\mathrm{m}^{-1}$, corresponds to the orange lines in figure 2.9a. It is higher as the first peak, because there are more orange features than black ones, providing more statistics.

The MFA is calculated by a two step procedure which is presented in figure 2.9. First, α is determined from the FFT of the AFM image and the tilt of the fiber with

respect to the vertical axis (β) from an optical image (see section 3.3). Finally, the MFA is determined by the relation

$$MFA = \alpha - \beta. \tag{2.9}$$

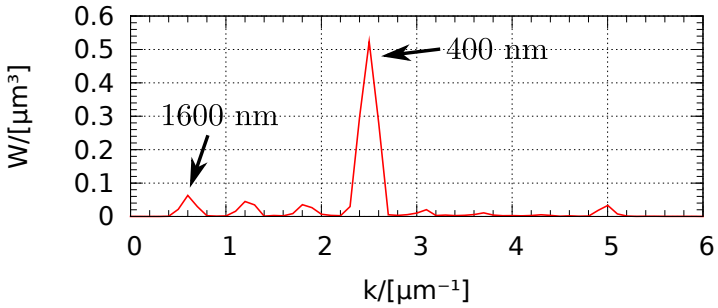

Figure 2.8: 1D PSD from figure 2.9a at angle α. 400 nm is the periodicity of the orange lines and 1600 nm of the black lines in figure 2.9a.

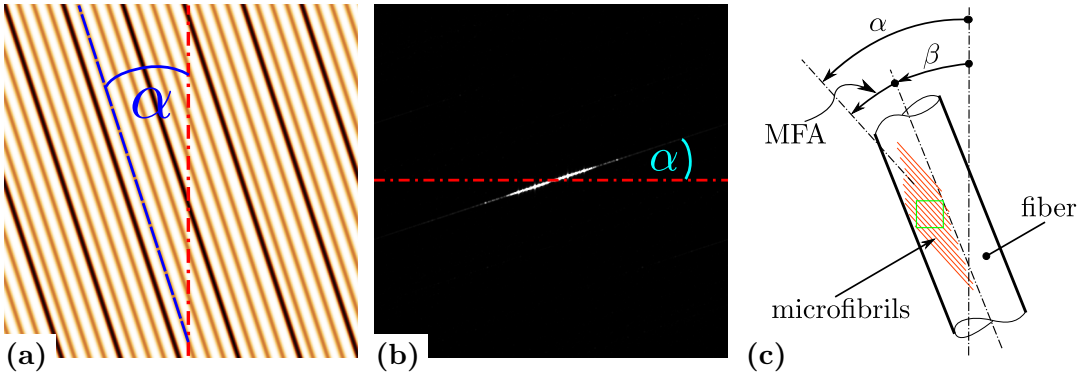

Figure 2.9: Schematic representation of an (a) 10 μm×10 μm AFM-image with oriented features, (b) its FFT and (c) the determination of the MFA. α–angle of microfibrils in the AFM image, β–tilt of the fiber with respect to the vertical axis. The green square marks the schematic representation in (a).

The Gwyddion software also allows the use of a so called watershed algorithm, which is able to detect grains on a surface. This algorithm can segment the image and mark grains by inverting the image in z-direction and finding local minima. The watershed algorithm works in two steps. The first step is to place a virtual water drop on every point of the inverted surface. If the drop was not placed at a local minimum, it follows the steepest slope until a minimum is found. The second step is to place more drops on the surface and find the grain boundaries by filling up the minima [41]. The algorithm tends to mark also regions on the surface, which are not the grains of interest but other local minima due to surface topography. These regions have to be removed manually for further evaluation. In this work, the watershed algorithm was used to determine the size

distribution of precipitates on fiber surfaces by calculating the equivalent disc radius from the areas of the marked precipitates [45]. The equivalent disc radius is the radius of a disc with the same area as the marked grain. The calculation of the equivalent disc radii and their distribution is also implemented in Gwyddion. To describe the precipitate size distribution quantitatively, the determined distribution is fitted with a Gaussian function $g(x)$, of the form

$$g(x) = n_0 \cdot e^{-\left(\frac{x-x_0}{s}\right)^2}. \tag{2.10}$$

Where x denotes the grain size, n_0 the frequency of grain sizes at the mean value x_0, and s the width of the distribution.

To quantify an asymmetric particle size distribution, the lognormal distribution $l(r)$ was fitted to the experimental data. The lognormal distribution is given by

$$l(r) = n_0 \cdot e^{-\frac{(\ln r - \ln r_0)^2}{(\ln s)^2}}. \tag{2.11}$$

In equation 2.11, n_0, r_0, and s describe the maximum of the distribution, the value of the particle radius at the maximum of the distribution, and the geometric standard deviation respectively [46].

The fit of the Gaussian function as well as the lognormal distribution to the experimental data was calculated by applying the Levenberg-Marquardt algorithm [43,44].

3 Experimental

3.1 Sample treatment

3.1.1 Native cellulose fibers

The native cellulose fiber samples were provided by Mondi where all treatments were performed. The samples were shipped as never dried pulp in three main forms: industrial kraft pulp [10] (called Monopol by Mondi and is a mixture of spruce and pine fibers), pure spruce kraft pulp, and pure pine kraft pulp. Spruce and pine kraft pulps were prepared in the laboratory and the industrial kraft pulp was taken from the actual manufacturing process.

The Monopol pulp was not further treated, and the difference of surface morphology between wet and dry native cellulose fibers was investigated.

The spruce and pine samples are unbleached and unrefined kraft pulp fibers. They were cooked in the laboratory to a kappa number of 39. After cooking, four different samples were prepared from the pulp: one untreated sample and three samples heated in a rotating reactor at a consistency of 5%, a pH of 8.5 and an electrolyte conductivity of 14.4 $\frac{\text{mS}}{\text{cm}}$ for 1 hour. The used temperatures for the three treated samples were 80 °C, 100 °C and 120 °C, where one temperature corresponds always to only one sample. Table 3.1 summarizes the treatment of the investigated pulps.

Table 3.1: Treatment of investigated pulp samples. $\langle d \rangle$ describes the average diameter of the investigated fibers, determined via optical microscopy (OM).

Sample	Number	$\langle d \rangle$ [μm]	bleached/refined	Treatment
Monopol	1	45±6	no/no	untreated
Spruce	4	46±9	no/no	untreated, 80 °C, 100 °C, 120 °C
Pine	4	43±7	no/no	untreated, 80 °C, 100 °C, 120 °C

3.1.2 Regenerated cellulose fibers

The regenerated cellulose fiber samples were provided by Kelheim Fibres GmbH and are all viscose type fibers, taken from the production cycle. All provided fibers were already cut to a length of 6 mm.

Bellini and Cellini fibers are hollow and collapsed. Therefore they offer a very flat and broad surface, which is ideal for AFM investigations. The difference between Bellini 1 and Bellini 4 fibers is, that when formed into a sheet, Bellini 1 shows a high breaking length but a low number of double folds whereas Bellini 4 shows a low breaking length and a high number of double folds. Cellini fibers are Bellini 4 fibers with CMC added during the spinning process to the viscose solution in liquid form. Classic viscose, in contrast to Bellini and Cellini, are not hollow and have a cloud shaped, curved cross-section. The two classical viscose samples differ in their stretching, one sample is only 5% stretched (low stretched), whereas the other sample is 40% stretched (high stretched). Table 3.2 lists the investigated regenerated cellulose fiber samples and their differences. Figure 3.1 presents the difference between the cross-sections of classical viscose fibers and Bellini (or Cellini) fibers.

Table 3.2: Specifications of investigated regenerated cellulose fibers. $\langle d \rangle$ describes the average diameter of the investigated fibers, determined via OM.

Sample	$\langle d \rangle$ [μm]	Cross-section	Treatment
Bellini 1	54±2	hollow and collapsed	untreated
Bellini 4	46±1	hollow and collapsed	untreated
Cellini	45±3	hollow and collapsed	CMC added
classical viscose 5% stretched	16±2	cloud-shaped	stretched
classical viscose 40% stretched	20±2	cloud-shaped	stretched

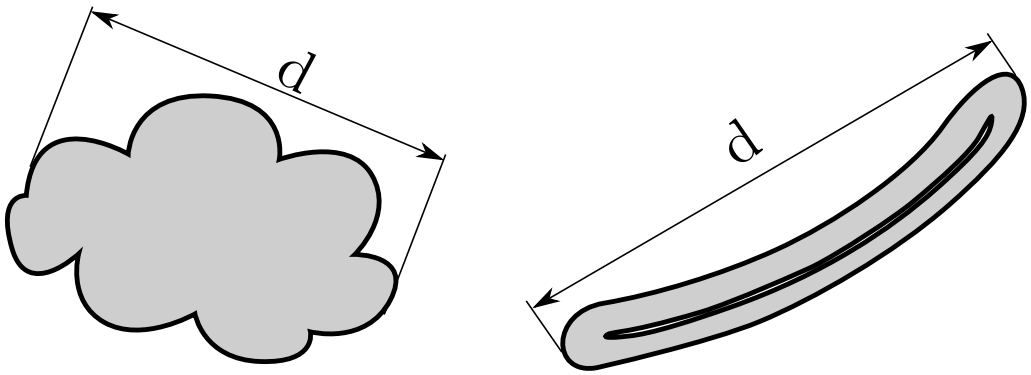

(a) **(b)**

Figure 3.1: Schematic cross-sections of (a) a classic viscose fiber and (b) a Bellini/Cellini fiber.

3.2 Sample preparation

3.2.1 Native cellulose fibers

In order to characterize the fiber surfaces of native cellulose fibers in the state where a paper sheet is formed, the samples had to be kept wet constantly. To ensure that the fibers would not dry, the already established preparation method for measurements under ambient conditions [36,37] had to be expanded.

The never dried pulp fibers were prepared on a randomly scratched silicon substrate, which was glued to a steel sample holder with nail polish. The random scratches were used as an aid to find the measured position again and to distinguish between two positions on the fiber. Usually, more than one measurement was performed on one fiber sample. Also the fiber itself was bonded to the silicon surface using nail polish. Because the measurement was not always carried out immediately after the preparation of a sample, a droplet of distilled water on the fiber prevented it from drying. A fully prepared sample is shown in figure 3.2 and the whole process of preparation is illustrated in figure 3.3.

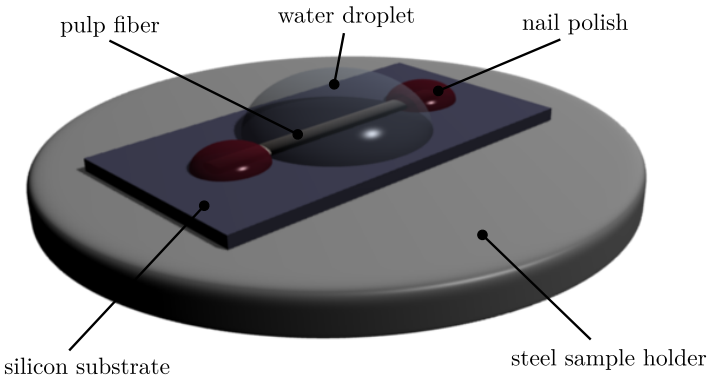

Figure 3.2: Principle of a prepared sample of a never dried pulp fiber, ready for investigation.

To extract a single fiber from pulp, a pulp chunk was placed into a water drop of sufficient size. Coarse tweezers were used to hold the chunk and with fine tweezers single fibers were pulled out in a way that they could be picked up easily, as depicted in figure 3.3a. Beforehand, a silicon substrate on a sample holder with a small water droplet was prepared (figure 3.3b). The extracted fiber was placed on the substrate, so that it was mostly covered with water. Only its very ends were sticking out, as it is presented in figure 3.3c. Nail polish was then used to bond the fiber at the ends to the silicon surface (figure 3.3d). It proved to be sufficient for the nail polish to harden for about 15 min. During this time, the small water droplet could evaporate and letting the fiber dry completely. Therefore, additional water had to be provided constantly with a syringe during the curing time of the nail polish.

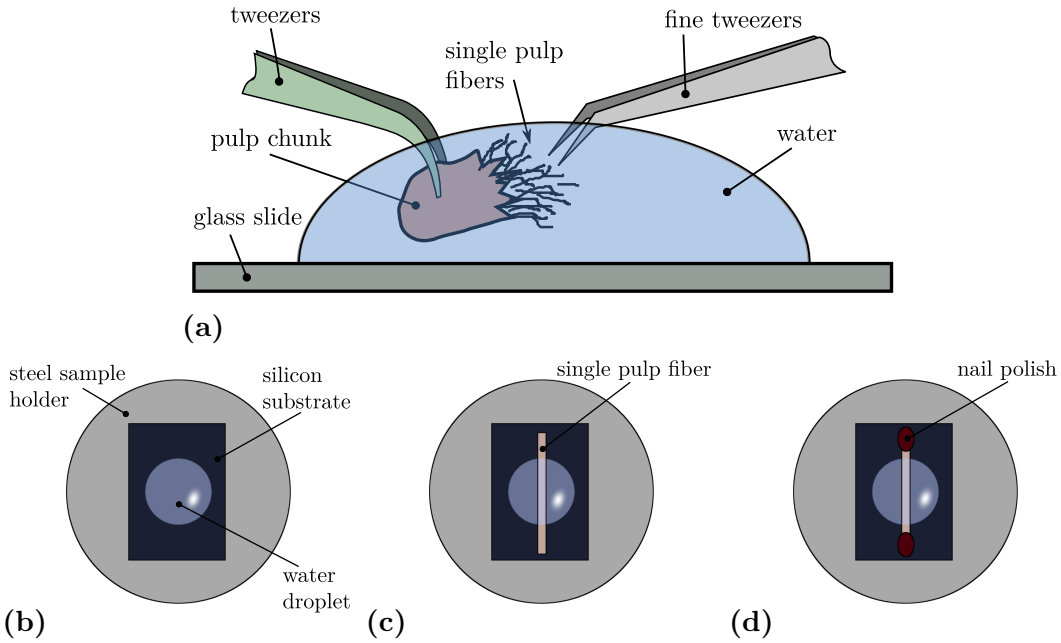

Figure 3.3: Schematic sample preparation of single pulp fibers for measurements in liquid media. (a) Extraction of a single fiber from pulp in water. (b) A water droplet on the silicon substrate. (c) Placing the fiber within the droplet. (d) Bonding of the fiber ends using nail polish.

After measuring the pulp fiber in water, it was dried for at least 30 min in air and measured again, now under ambient conditions.

3.2.2 Regenerated cellulose fibers

The regenerated cellulose fiber samples were measured only under ambient conditions and the fibers arrived at the laboratory in Leoben separated from each other, so the preparation was simpler than in the case of the wet pulp fibers. Again, the fiber was bonded on a randomly scratched silicon substrate but this time the substrate was fixed to the sample holder with double sided adhesive tape. For pulp fibers, nail polish was used to bond the fibers on the silicon substrate, because the glue on the adhesive tape would be dissolved in water. However, the regenerated cellulose fiber samples were only measured under ambient conditions, allowing the use of single sided adhesive tape to bond the fibers on the substrate. The advantages of adhesive tape over nail polish are that it is easier to handle and does not need time to cure. The setup is displayed schematically in figure 3.4.

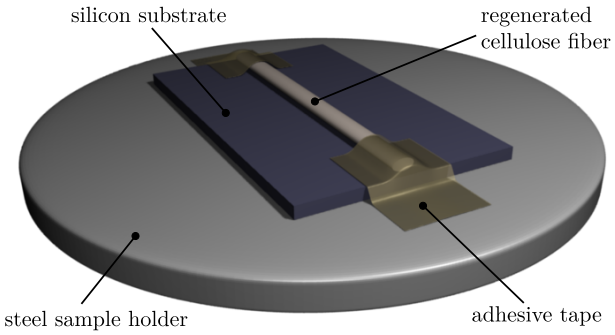

Figure 3.4: Scheme of a prepared sample with a regenerated cellulose fiber.

3.3 AFM Setup

For all measurements reported here, the used AFM was an Asylum Research MFP 3D AFM, presented in figure 3.5. This instrument is equipped with a closed loop scanner, which means that the actual movement of the piezoelectric actuator is monitored by a sensor. In the Asylum Research MFP 3D AFM an inductive sensor is used. With this setup an online correction of the expansion or contraction of the piezoelectric actuators by a feedback loop is possible.

To investigate pulp fibers in water, the AFM was equipped with a fluid cell, which is described in detail in section 3.4. Fully prepared dried pulp fiber samples and regenerated fiber samples were fixed on a glass slide and placed on the sample stage of the AFM.

The Asylum Research MFP 3D AFM allowed a sufficient z-range to measure $10\,\mu\text{m}\times10\,\mu\text{m}$ images on pulp fibers (dry and wet) and up to $20\,\mu\text{m}\times20\,\mu\text{m}$ images on all collapsed hollow regenerated viscose cellulose fibers (Bellini, Cellini). Classic viscose fibers allowed only $10\,\mu\text{m}\times10\,\mu\text{m}$ images, because their surface was too rough and their diameter too small.

The samples were placed in the AFM in a way that the fiber axis was approximately perpendicular to the cantilevers long axis which is also the fast scanning axis (presented in figure 3.6).

From every measurement an optical image was taken which allowed to measure the angle between the fiber axis and the long axis of the cantilever. With this information it was then possible to measure the microfibril angle with respect to the main fiber axis.

Figure 3.5: Photograph of an Asylum Research MFP 3D AFM.

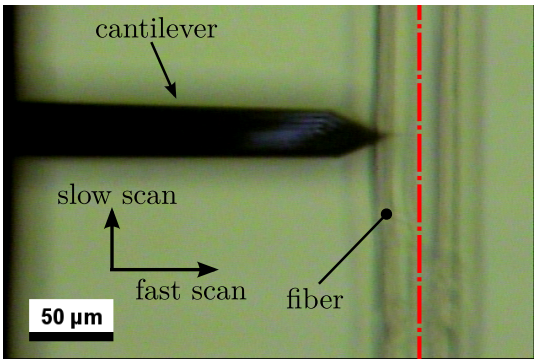

Figure 3.6: Optical image of an AC240TS cantilever scanning on a pine fiber in liquid. The red line marks the main fiber axis.

3.4 Fluid Cell

Preliminary measurements were done with a Digital Instruments Nanoscope IIIa AFM, equipped with an open liquid cell. This setup, however, allowed stable conditions only for 1 hour, since the cell is completely open. Because of that, only very small droplets could be used, to avoid damage of the piezo scanner by spilling water over it. The second limitation on this system is the range of the z-piezo of about $4\,\mu$m. These two restrictions allowed to record images only up to a maximum size of $5\,\mu\text{m}\times5\,\mu$m images, since larger images take more time to measure and also need an increased z-range (due to fiber curvature), which could not be provided by this system.

To measure images of $10\,\mu\text{m}\times10\,\mu$m image size, the Asylum Research MFP 3D AFM was chosen, due to its higher z-range. The system is equipped with an Asylum Research Closed Fluid Cell (see figure 3.7) that allowed safe measurements of the fibers in water for several hours. The used operation mode of the fluid cell was in an open

configuration, which allowed more flexibility than the closed configuration. In the open configuration the bottom part of the fluid cell is completely sealed, whereas the membrane is only fixed at the cantilever holder but not clamped to the bottom part. This configuration combines the advantage of an easy setup and fast access to the sample with the protection of the piezo stage, by using only a low amount of liquid.

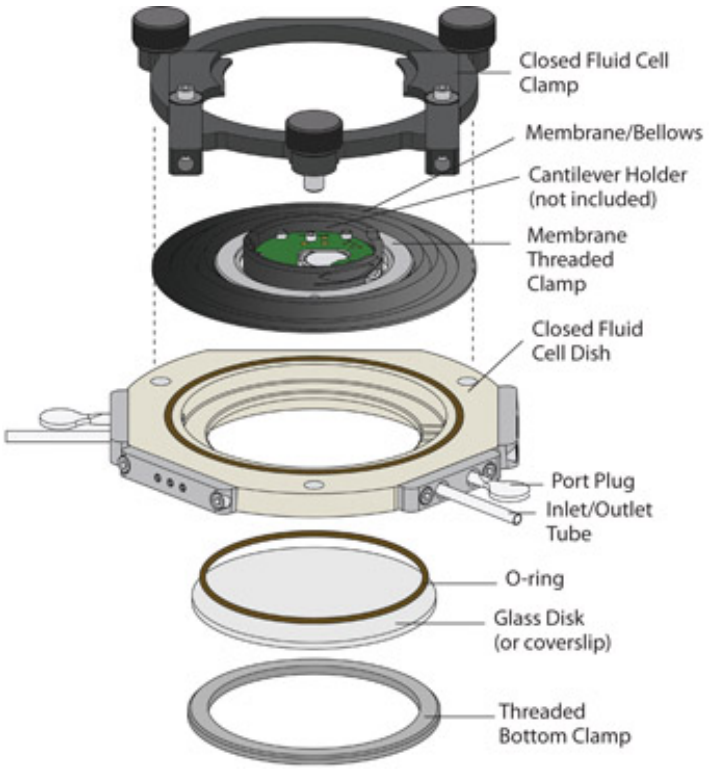

Figure 3.7: Schematical drawing of an Asylum Research Closed Fluid Cell. (From [47].)

The sample was fixed to the glass disk on the bottom with double sided adhesive tape. A water droplet was placed over the sample to cover the sample completely (see figure 3.8). That setup ensured stable conditions for at least six hours, though a point of instability, due to complete evaporation of the liquid, was never reached.

During the approach of the cantilever to the sample surface, it is diving into the water, which is wetting the cantilever holder and forming a meniscus, as presented schematically in figure 3.9. In this process, a stable liquid environment is formed around the sample, without the need of flooding the whole fluid cell.

When measuring in liquids, the cantilever tuning becomes more complicated. Problems arise, because not only the cantilevers resonance frequency is shifted towards lower values, but also the oscillation amplitude is dampened considerably and side-peaks from the fluid cell appear. The resonance curves of a cantilever in water and in air are displayed in figure 3.10.

For this reason a thermal sweep is performed first and appended to the resonance

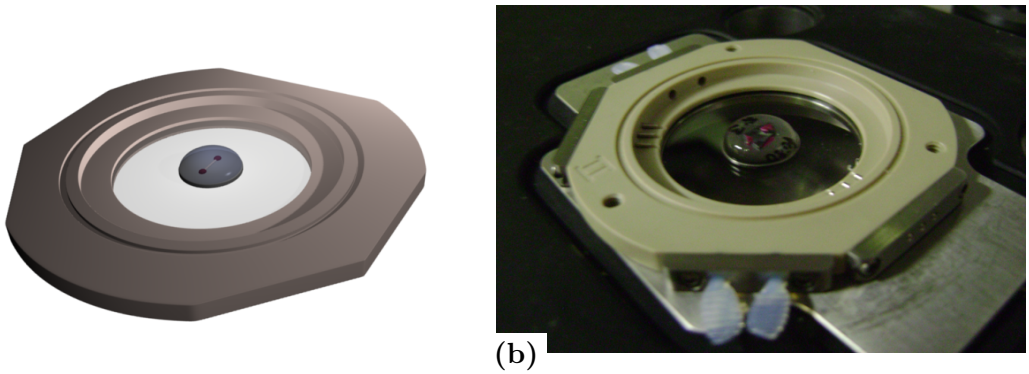

(a) (b)

Figure 3.8: Prepared sample fixed on the fluid cell with a water drop on it. (a) Schematic and (b) photograph of real setup.

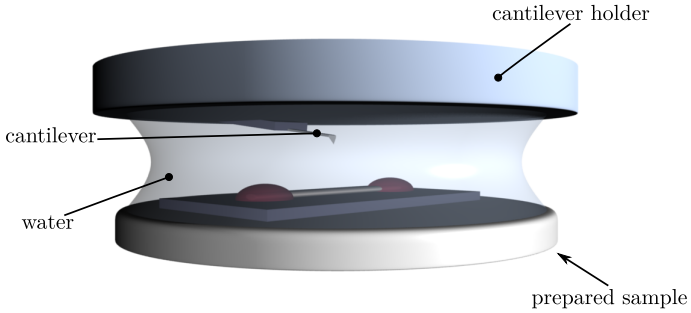

Figure 3.9: Scheme of a stable liquid environment after approaching the AFM tip to the sample surface in side view presentation.

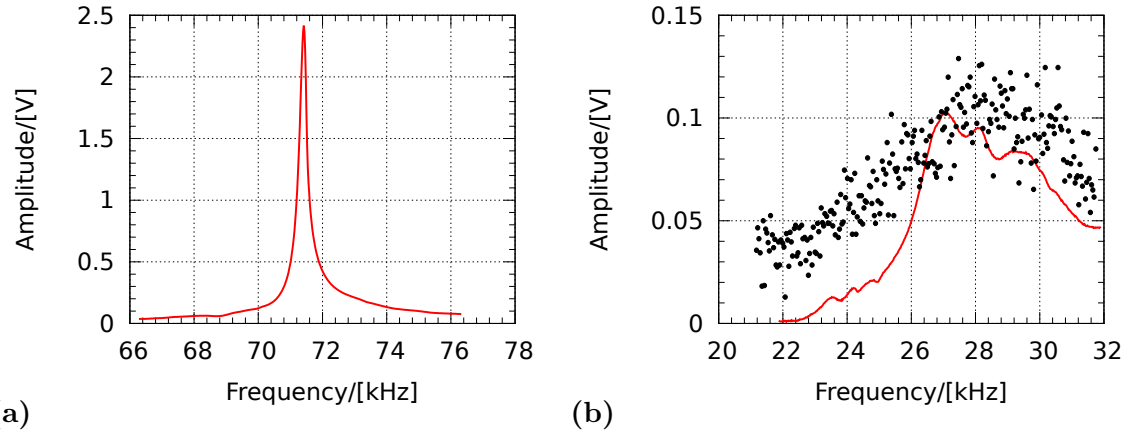

(a) (b)

Figure 3.10: Resonance curves of an AC240TS cantilever (a) in air and (b) in water. The black dots are data points from a thermal sweep.

curve. The thermal sweep shows the resonance peak of the cantilever and the resonance curve in water corresponds to the whole system. With this, it is possible to select a

peak near the real resonance frequency. The resonance peak in water does not have to be very sharp at first and a target amplitude of only 100 mV is sufficient. A low target amplitude is necessary in water to keep the voltage of the piezo – that oscillates the cantilever – low. To increase sensitivity, the resonance peak can be enhanced by a Q-gain in the range of 0.9–1.1, which leads then to a sharp peak and a high amplitude of about 700 mV.

3.5 AFM Probes

Probes used for this work were Olympus AC240TS, AC160TS and BioLeverMini BL-AC40TS. All of them are tapping mode probes, but the BL-AC40TS are especially designed for use in liquid environments. Besides cantilever geometry, the BioLeverMini are differing from the other probes in cantilever material (silicon tip on silicon nitride lever instead of silicon tip on silicon lever) and tip geometry (5° side angle instead of 15°), details are shown in tables 3.3 and 3.4. The best choice for measurements in water with a size of 10 μm × 10 μm were AC240TS probes. The resulting fiber surface roughness on that scale led to increased instability for the very soft BL-AC40TS cantilevers.

Table 3.3: Tip specifications of the used probes. (From [48].)

probe	material -	shape -	radius [nm]	height [μm]	angles front [°]	angles back [°]	angles side [°]
AC240TS	Si	3-sided	9 ± 2	14 ± 4	0 ± 1	35 ± 1	15 ± 1
AC160TS	Si	3-sided	9 ± 2	11 ± 4	0 ± 1	35 ± 1	15 ± 1
BL-AC40TS	Si	3-sided	9 ± 2	7 ± 2	5 ± 1	35 ± 1	5 ± 1

Table 3.4: Cantilever specifications of the used probes. (From [48].)

probe	material -	resonance [kHz]	spring [$\frac{N}{m}$]	length [μm]	width [μm]	thickness [μm]
AC240TS	Si	50 - 90	0.5 - 4.4	230 - 250	28 - 32	1.7 - 3.7
AC160TS	Si	200 - 400	12 - 103	150 - 170	48 - 52	3.6 - 5.6
BL-AC40TS	Si_3N_4	50 - 350	0.05 - 1.2	28 - 48	15 - 17	0.15 - 0.25

All probes have a tetrahedral tip located at the very end of the cantilever, which is visible in figure 3.11. This allows an exact positioning on the sample surface under the optical microscope attached to the AFM.

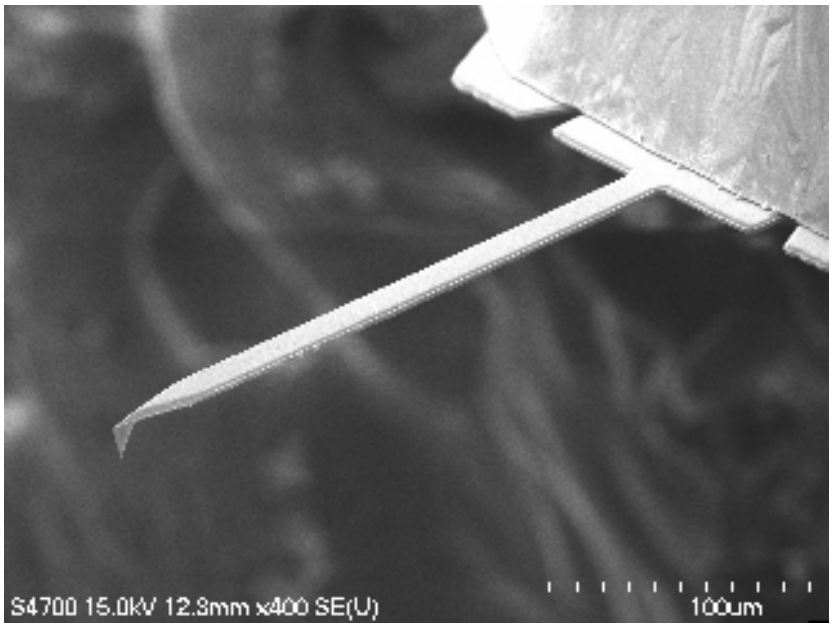

Figure 3.11: Scanning electron microscopy (SEM) image of an AC240TS. (From [49].)

4 Results

4.1 Wet and dry native cellulose fibers

4.1.1 Differences between wet and dry softwood pulp fibers

First AFM measurements were performed to investigate the morphological difference between wet and dried softwood pulp fibers. The samples were extracted from a Monopol kraft pulp which is a mixture of spruce and pine fibers. Therefore, it is not possible to specify the type of fiber that was inspected. Figure 4.1 shows a $10\,\mu\text{m}\times10\,\mu\text{m}$ AFM height image of a softwood fiber surface measured in water. On the surface, there are several features visible: two microfibril bundles – one horizontal and another vertical oriented – and individual single microfibrils are also resolved. Although the surface appears in figure 4.1 rather smooth, it has a high RMS roughness σ of 220 nm.

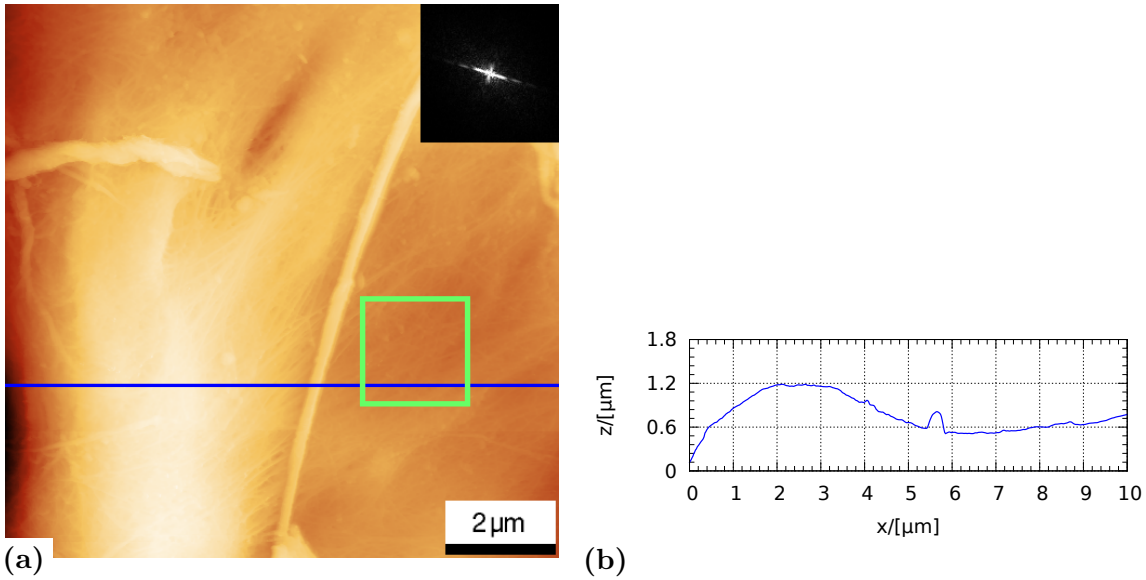

(a) (b)

Figure 4.1: $10\,\mu\text{m}\times10\,\mu\text{m}$ AFM topography image of a softwood fiber surface, measured in wet state. (a) Height image, z-scale: 1500 nm, the green square indicates the position of figure 4.3a, the arrows mark microfibril bundles. The inset represents the 2D PSD of the AFM height image. (b) Line profile, its position is marked by the blue line in (a).

Figure 4.2 presents an image measured on the same pulp fiber as in figure 4.1a but after drying of the fiber. A completely different surface appearance is visible after drying of the fiber. The surface is now heavily wrinkled with a wrinkle size of $529\,\text{nm}^{+157\,\text{nm}}_{-99\,\text{nm}}$

(from PSD section) and 497 nm±135 nm (measured from the line profile). The surface roughness σ of the scanned area in figure 4.2a is 185 nm, which is lower than the value obtained from the AFM height image measured in water. It is important to note that microfibrils are not recognizable in the height image, in a dry fiber state.

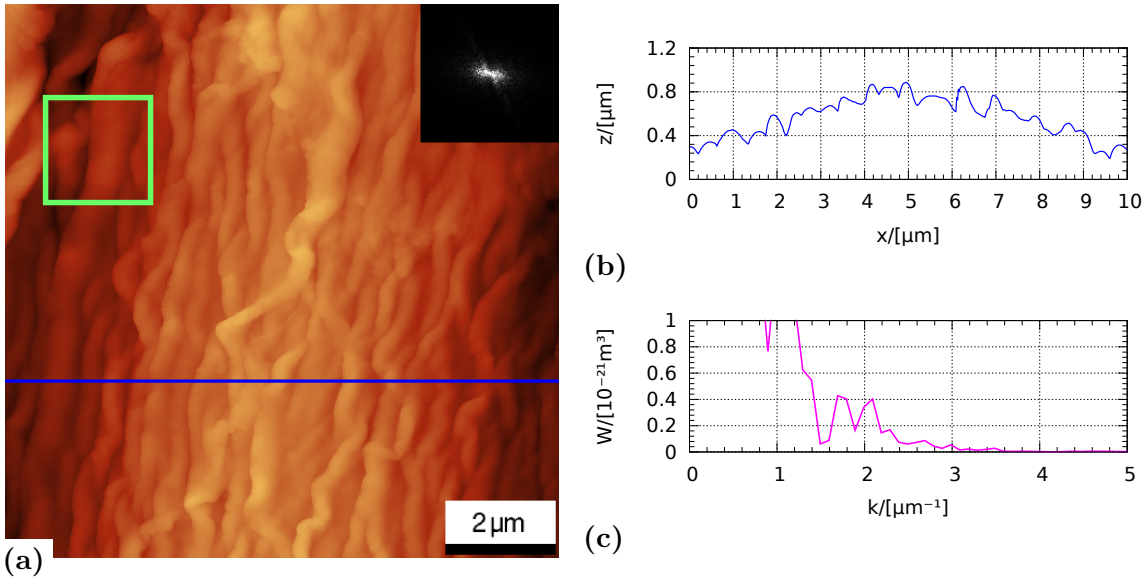

Figure 4.2: 10 μm×10 μm AFM image of a softwood fiber, measured in air. (a) Height image, z-scale: 1500 nm, the green square indicates the position of figure 4.3b. The inset represents the 2D PSD of the AFM height image. (b) Line profile, its position is marked by the blue line in (a). (c) PSD section at -19° with respect to the k_x-axis.

As discussed for figure 4.1 and figure 4.2 the surface roughness σ is higher for the scanned region of the pulp in the wet state. Here, the local curvature of the surface is heavily influencing σ and depends on measured fiber position. However, the main difference between wet and dry fibers are the surface wrinkles. The surface wrinkles cannot be used to quantify the difference of wet and dried fibers from 10 μm×10 μm AFM height images because fiber curvature occurs in both states on this scale and overlays the influence of the finer structures. Therefore, figure 4.3 represents 2 μm×2 μm images of a fiber surface measured in wet (figure 4.3a) and dry (figure 4.3b) state. It is clearly visible that the wet fiber surface is rather smooth with low fluctuations in height corresponding to the height of single fibrils, whereas the dried fiber surface has higher height fluctuations leading to a RMS roughness of 16 nm and 68 nm respectively. The microfibrils in the scanned region in figure 4.3a show no preferred orientation and are 41 nm±12 nm wide. From the 2D PSD in figure 4.3a, also no single orientation of the microfibrils is visible. This lack of a preferred orientation leads to the conclusion that the investigated layer is the P layer.

Further investigations of 2 μm×2 μm images obtained from 5 independent positions were first measured in water and after the fiber has dried. The positions were randomly chosen on the fiber that the scanned areas are not overlapping. These measurements resulted in an average RMS roughness of 37 nm±11 nm for the wet fiber and 73 nm±39 nm

for the dried fiber. In table 4.1 the single values of the measured RMS roughness are shown, indicating that dry fibers can also have a low roughness but are in general rougher than wet fibers at that scale.

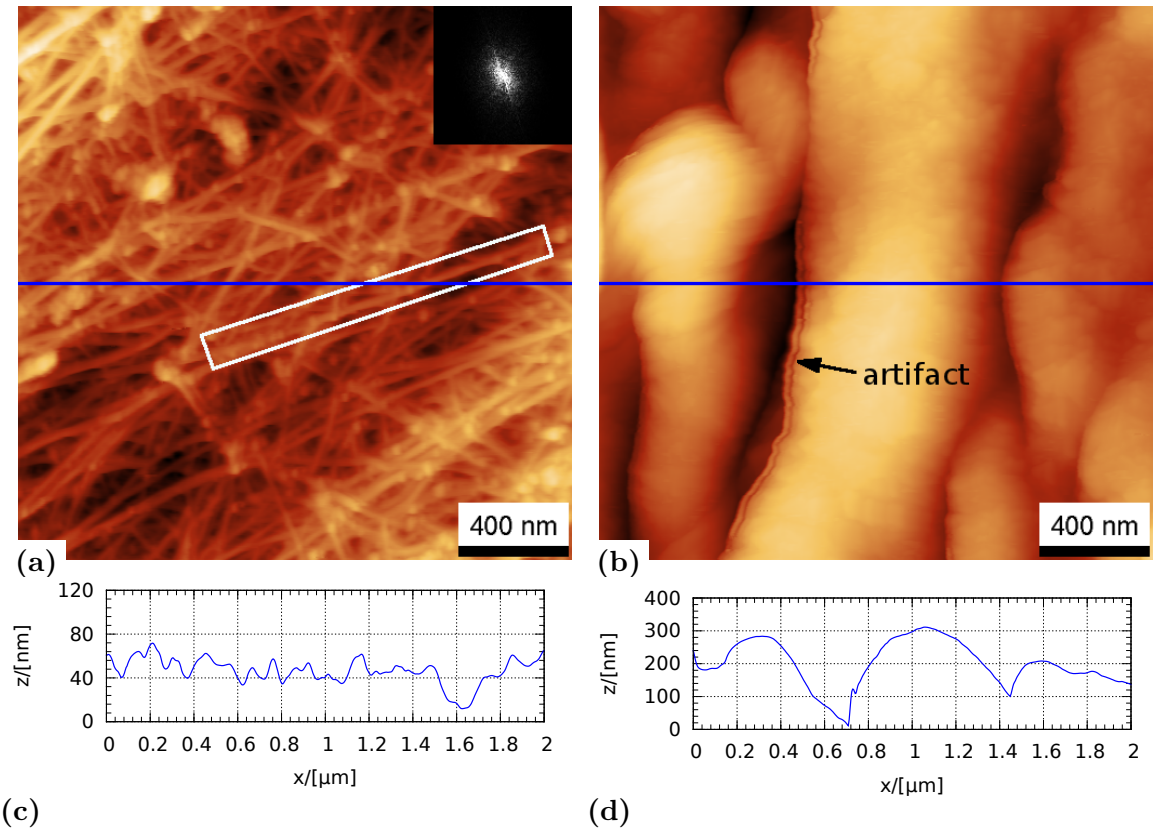

Figure 4.3: $2\,\mu$m$\times 2\,\mu$m AFM topography images of a softwood fiber surface. (a) Height image, measured in water, z-scale: 120 nm. The white rectangle encircles a single microfibril. The inset represents the 2D PSD of the AFM height image.(b) Height image, measured in air, z-scale: 400 nm. (c) Line section of (a). (d) Line section of (b). The position of the line sections is indicated by the blue lines in the AFM images.

Table 4.1: RMS roughness values (σ) from wet and dry softwood fibers in [nm], calculated from $2\,\mu$m$\times 2\,\mu$m AFM height images.

wet/dry	Position 1	Position 2	Position 3	Position 4	Position 5	mean value
wet	46	26	28	34	51	37 nm±11 nm
dry	32	74	63	136	60	73 nm±39 nm

4.1.2 Spruce

Untreated pulp

Figure 4.4 shows a 10 μm×10 μm AFM height image of a spruce fiber surface measured in water. The pulp, from which this fiber was extracted, did not receive any temperature treatment and serves therefore as an untreated reference sample. In the height image (see figure 4.4a) the microfibrils are clearly visible. Using PSD analysis, the width of the microfibrils was calculated to be $125\,\mathrm{nm}^{+14\,\mathrm{nm}}_{-11\,\mathrm{nm}}$ and a manual measurement from a line profile perpendicular to the fibril orientation resulted in a microfibril width of 172 nm±65 nm.

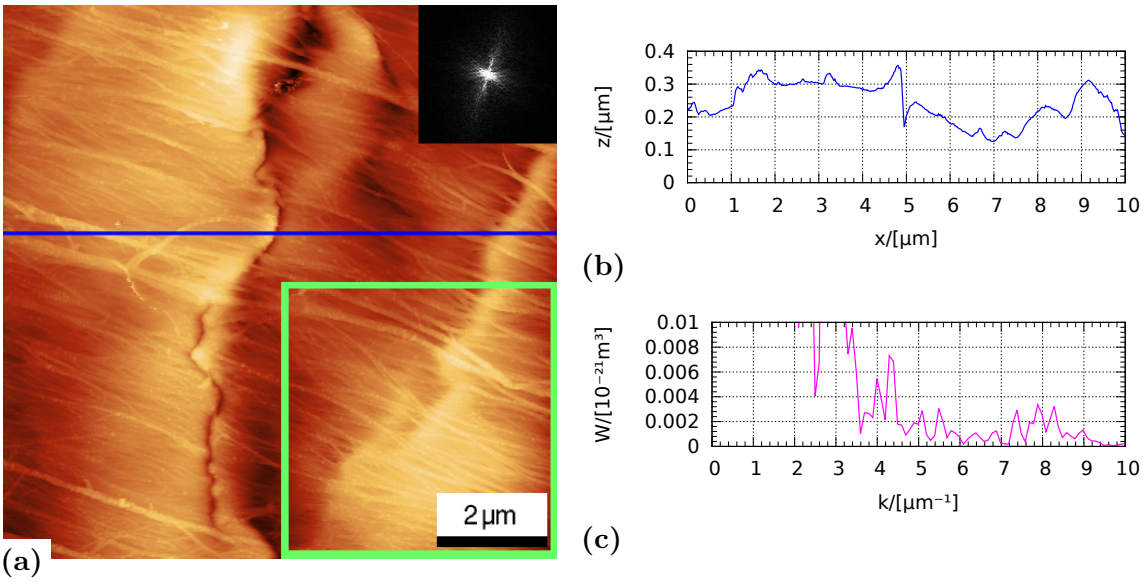

Figure 4.4: 10 μm×10 μm AFM height image of an untreated spruce fiber surface, measured in water. (a) Height image, z-scale: 500 nm, the green square indicates the position of figure 4.5. The inset represents the 2D PSD of the AFM height image. (b) Line profile, its position is marked by the blue line in (a). (c) PSD section at 73° with respect to the k_x-axis.

From the 2D PSD and an optical image of the fiber, the MFA was calculated to be 78°, which strongly suggests the assumption that the measured layer is the S1 layer. The AFM image also shows surface wrinkles running perpendicular to the fibril orientation and a narrow trench running vertically through the image. The trench seems to be caused by two surface wrinkles overlapping, forming a V-shaped valley with microfibrils bridging over it. A microfibril bundle bridging the two sides is observed best on the upper part of the image in figure 4.4a, where the trench is wider. In the line profile in figure 4.4b, the shape of the trench is visible at around 5 μm. The RMS roughness of the surface is 70 nm.

The high-resolution image in figure 4.5 shows lignin precipitates on the microfibrils. The microfibril size is $119\,\mathrm{nm}^{+3\,\mathrm{nm}}_{-3\,\mathrm{nm}}$, determined from the PSD section. The manual evaluation of a line profile perpendicular to the fibril orientation yields a microfibril size of

128 nm±31 nm. These values are comparable to those extracted from the 10 μm×10 μm AFM height images, which confirms that the microfibril size can be measured from 10 μm×10 μm AFM images with the advantage of more statistics.

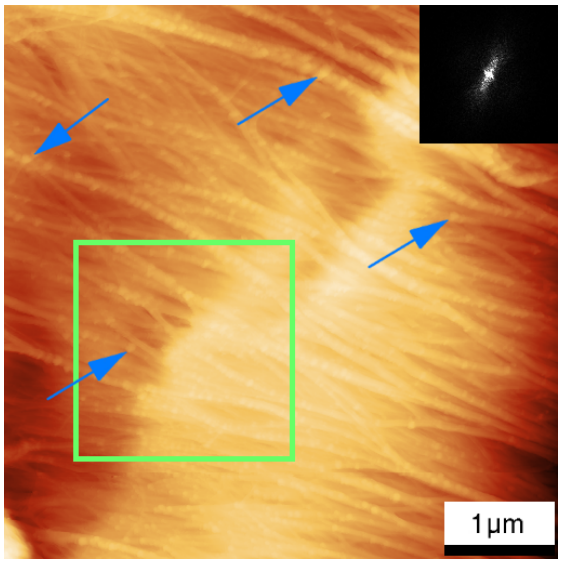

Figure 4.5: 5 μm×5 μm height image, z-scale: 400 nm. The green square indicates the position of the AFM image in figure 4.6. The arrows indicate lignin precipitates on the microfibrils. The inset represents the 2D PSD of the AFM height image.

For comparison, another 10 μm×10 μm image of the same fiber was recorded and evaluated. The microfibril size from PSD and manual determination is $132\,\mathrm{nm}^{+3\,\mathrm{nm}}_{-3\,\mathrm{nm}}$ and 147 nm±34 nm respectively, which is comparable to the values from the image in figure 4.4a. A measured MFA of 69° indicates that the S1 layer is observed.

To determine the average size of the lignin precipitates on the pulp fiber surface, a higher resolved 2 μm×2 μm AFM height image was measured. Here, the watershed algorithm from Gwyddion software was used to mark the precipitates. In order to apply this algorithm, the image was flattened as much as possible by the subtraction of a 12th order polynom in x- and y-directions. It is critical to subtract a polynomial background from an acquired image – especially if the polynom is of a high order – because not only unwanted height information will be subtracted from the acquired data, but also information that is needed to characterize the surface. In this case, a flattening with a 12th order polynom was adequate, because the watershed algorithm works best on very flat images and no other information besides grain size was obtained from images processed that way. The precipitate size was determined by calculating the equivalent disc radius [45]. This procedure led to an average precipitate diameter of 47 nm±17 nm. The AFM image is shown in figure 4.6a and the resulting size distribution of the lignin precipitates in figure 4.6b. The precipitates are found to always line up on a microfibril.

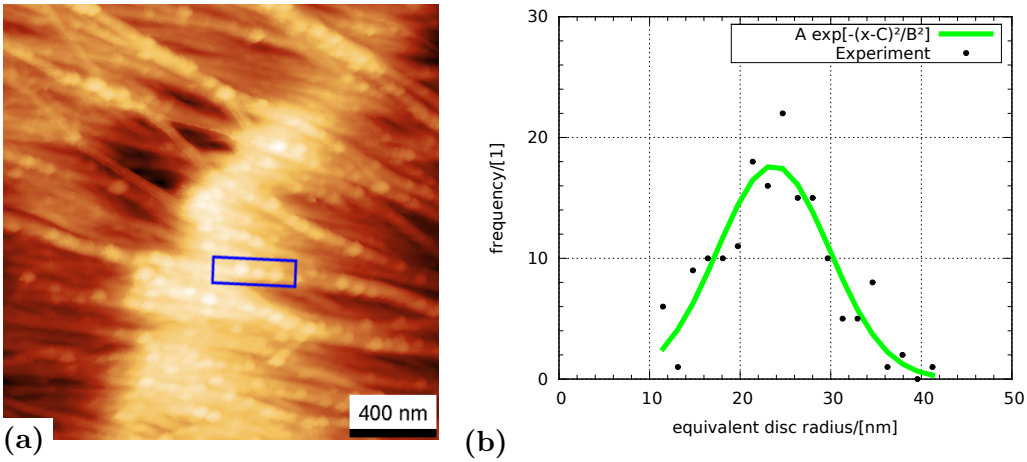

Figure 4.6: Lignin precipitates on an untreated spruce fiber. (a) 2 μm×2 μm height image, z-scale: 120 nm. The blue rectangle encircles three lignin precipitates which are characterized by a line profile in figure 4.7. (b) Size distribution of the lignin precipitates. The black dots are the data points determined from the experiment and the green line is a Gaussian fit.

Figure 4.7 presents a line profile of the three lignin precipitates marked in figure 4.6. The profile was leveled by subtracting a linear background to measure the heights of the precipitates. From left to right, the heights of the precipitates are 10 nm, 9 nm, and 13 nm. This procedure was carried out to determine the heights of 10 precipitates in figure 4.6, which lead to an average height of the lignin precipitates of 10 nm±3 nm.

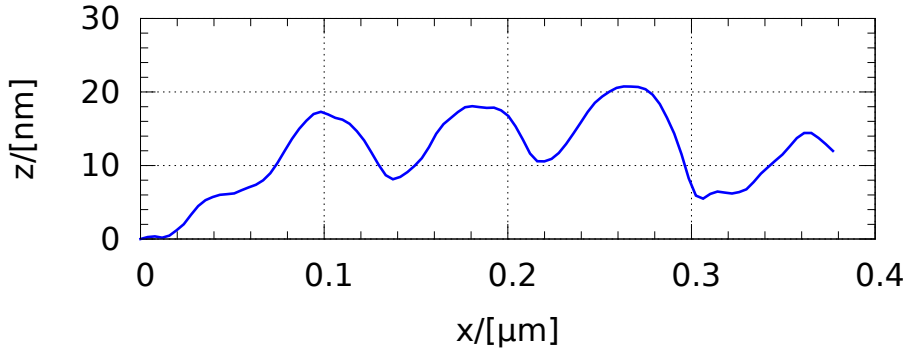

Figure 4.7: Leveled line profile of three lignin precipitates. The precipitates are marked by a blue rectangle in figure 4.6.

Temperature treated pulp (80°C)

Figure 4.8 represents a 10 μm×10 μm AFM height image of a pulp fiber surface after a heat treatment at 80 °C measured in water. The surface is still smooth, but no trench can be observed, instead there seem to be overlapping layers on the surface, which can be observed best on the right part of the scanned region. The border of the topmost

layer on the right part of the image is jagged and is for the most part oriented about 60° with respect to the x-axis. At the border of the layer, the surface is piled up, which is visible in the line profile (figure 4.8b) at the range of 5 μm to 6 μm. The borders of the layers could still be considered as surface wrinkles, but are certainly of a different kind as on the scanned surface areas of the other fibers. A surface morphology like displayed in figure 4.8a, was not observed on any of the other fibers, even a scan on a different fiber, but with the same temperature treatment showed a different morphology. On the left side of the image, a flat region can be seen, whereas the right part seems to be slightly curved. The microfibril size is $110\,\mathrm{nm}^{+3\,\mathrm{nm}}_{-3\,\mathrm{nm}}$ obtained from the PSD analysis and 110 nm±39 nm from manual determination. The observed RMS roughness of 109 nm is larger than the roughness obtained from the untreated sample, which can be explained by the curved fiber surface at the 80 °C treated fiber. The MFA of 66° indicates the observed fiber surface as the S1 layer.

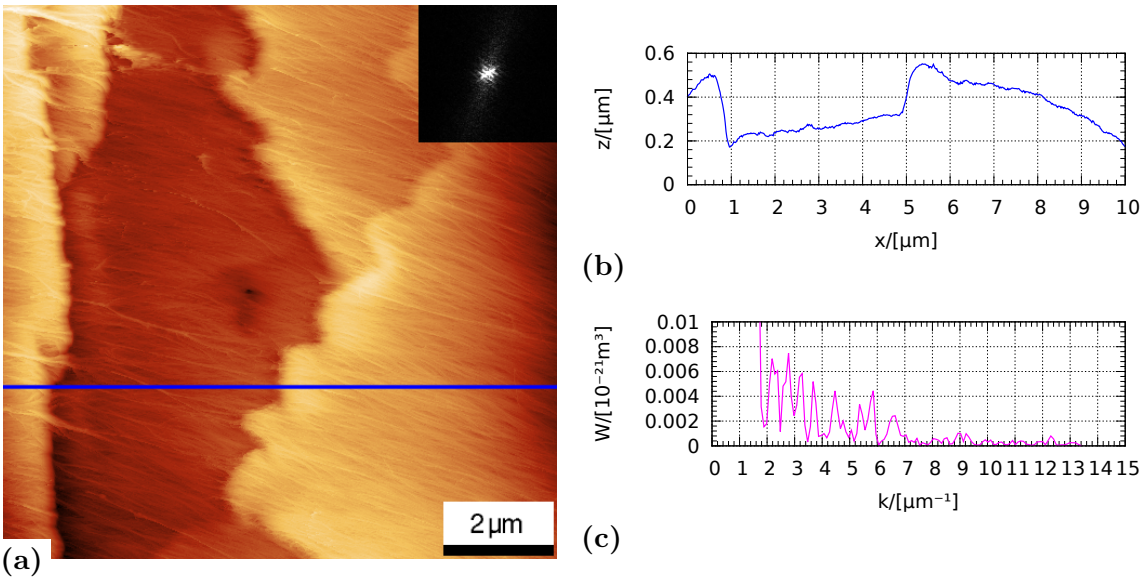

Figure 4.8: 10 μm×10 μm AFM height image of a spruce fiber treated at 80 °C, measured in water. (a) Height image, z-scale: 700 nm. The inset represents the 2D PSD of the AFM height image. (b) Line profile, the position is indicated by the blue line in (a). (c) PSD section at 63° with respect to the k_x-axis.

On the AFM image displayed in figure 4.8a, no lignin precipitates are visible, also higher resolved images did not show lignin precipitates. Another AFM image on a different fiber, but also from the 80 °C temperature treated pulp, showed lignin precipitates, but not as clear as the 2 μm×2 μm AFM height image scanned on the untreated fiber. The 2 μm×2 μm AFM height image is presented in figure 4.9a and the corresponding phase image in 4.9b. Here, the phase image provides a better contrast than the height image and allows to visualize the lignin precipitates. The precipitate size was, however, calculated from the height image, because the watershed algorithm did not work on this phase image. The lignin precipitate size distribution is displayed in

4.9c from which the average diameter of the lignin precipitates is determined to be 24 nm±10 nm.

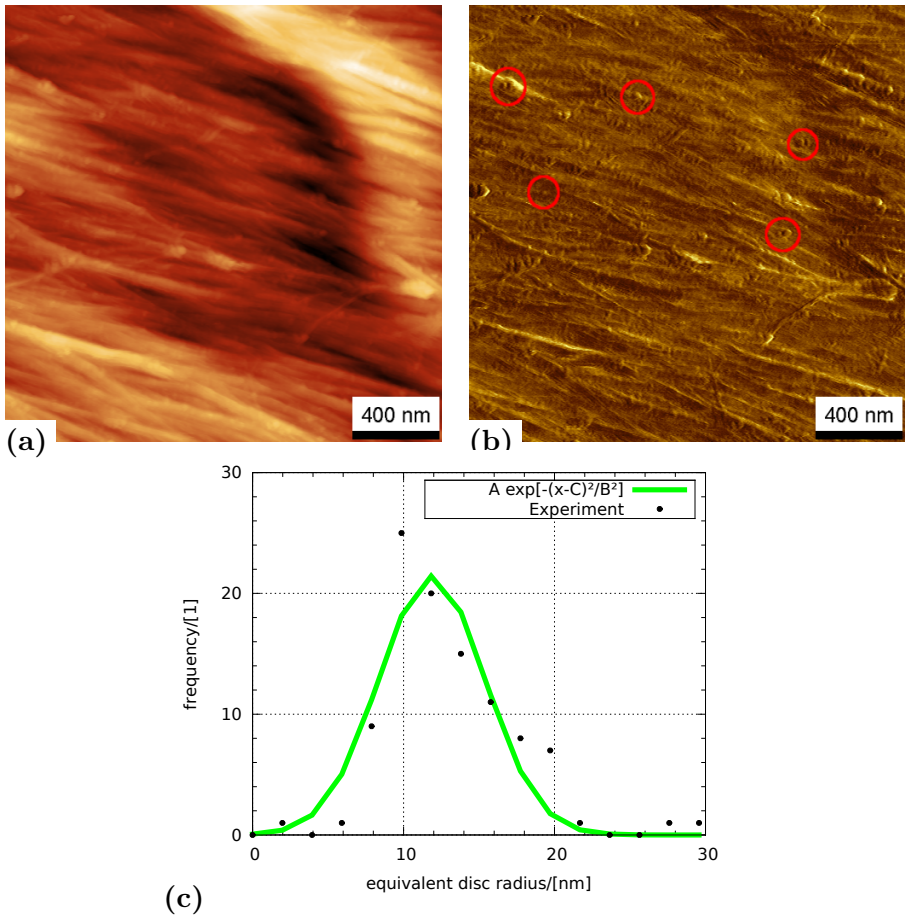

Figure 4.9: Lignin precipitates on an 80 °C treated spruce fiber. (a) 2 μm×2 μm height image, z-scale: 100 nm. (b) 2 μm×2 μm phase image, z-scale: 10°. The red circles mark lignin precipitates. (c) Size distribution of the lignin precipitates. The black dots are the data points determined from the experiment and the green line is a Gaussian fit.

Temperature treated pulp (100°C)

Analysis of figure 4.10 revealed an increase of microfibril bundles on the 100 °C treated pulp fiber surface. Besides that, the fibril bundles are more elevated from the cell wall than on the untreated and 80 °C treated pulp fibers.

The line profile in figure 4.10b indicates a surface that is flat, which leads to a low surface roughness of 56 nm. The RMS roughness of this scanned area is the lowest of all spruce fiber surfaces, because in the other images there is always an influence of the fiber curvature. This fiber curvature can be recognized in the line profiles. Further evaluation of the image yields a microfibril width of $137\,\mathrm{nm}^{+74\,\mathrm{nm}}_{-36\,\mathrm{nm}}$ from PSD analysis and

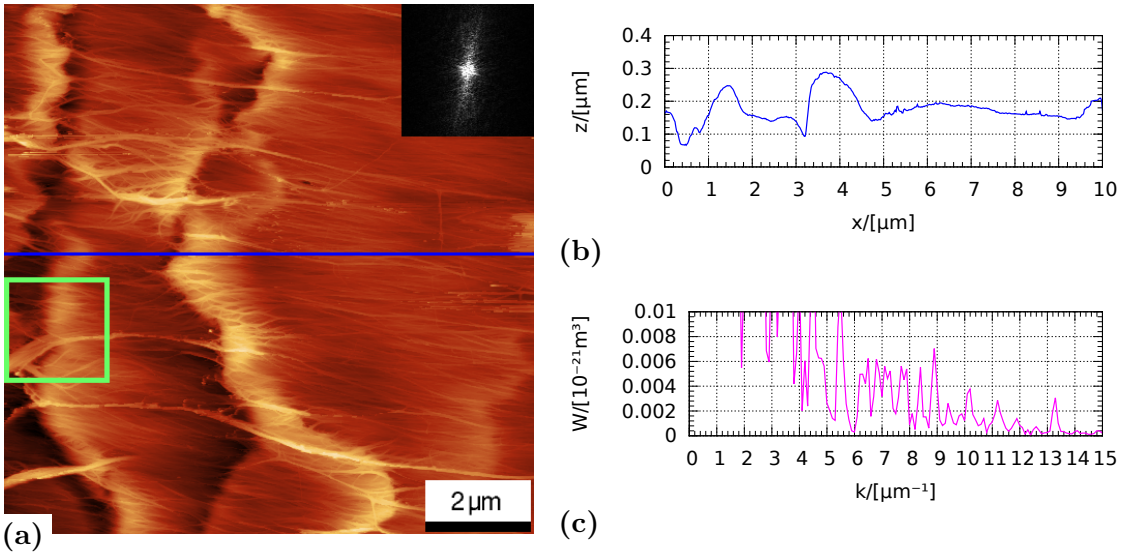

Figure 4.10: 10 μm×10 μm AFM height image of an 100 ℃ temperature treated spruce fiber, measured in water. (a) Height image, z-scale: 500 nm. The green square marks the position of the 2 μm×2 μm image in figure 4.11. The inset represents the 2D PSD of the AFM height image. (b) Line profile, the position is indicated by the blue line in (a). (c) PSD section at 77° with respect to the k_x-axis.

127 nm±45 nm from manual measurement, which is in the range of the other samples. The MFA is 80° and therefore the measured layer is again the S1 layer.

None of the images (recorded on two different fibers) showed lignin precipitates on them. This does not mean that there are no precipitates at all on the fiber surface, only that there were none at the measured positions. Figure 4.11a shows the microfibrils in the AFM height image, but no lignin precipitates are observed. Also the AFM phase image (figure 4.11b), which provides in this case better contrast, shows the microfibrils very well but there are no signs of lignin precipitates.

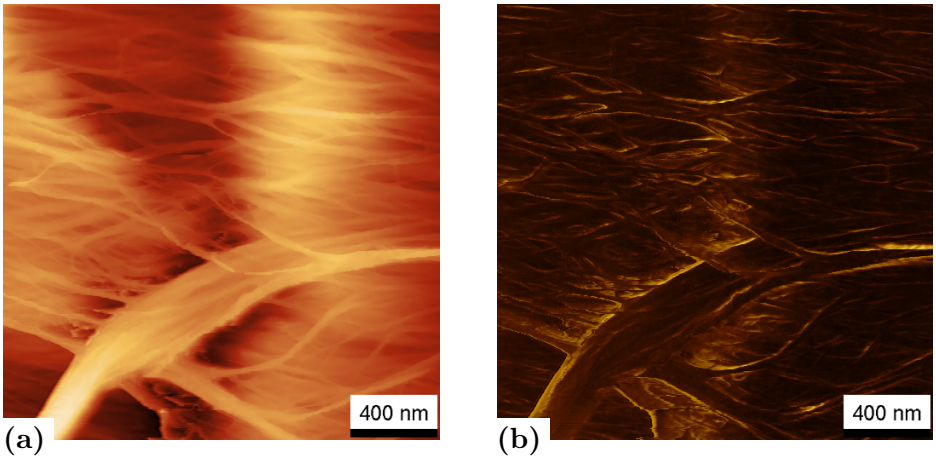

(a) (b)

Figure 4.11: 2 μm×2 μm image of an 100 ℃ temperature treated spruce fiber, measured in water. (a) Height image, z-scale: 400 nm. (b) Phase image, z-scale: 40°

Temperature treated pulp (120°C)

The surface morphology of the 120 ℃ treated pulp fibers (compare figure 4.12) looks similar to the 100 ℃ treated fibers. The RMS roughness of the surface is 93 nm, which is higher than the roughness of the 100 ℃ treated fibers, because the surface is not overall flat but has a slope on the left side of the AFM height image. Here, the determination of the microfibril width leads to $118\,\mathrm{nm}^{+8\,\mathrm{nm}}_{-7\,\mathrm{nm}}$ using PSD analysis and 133 nm±54 nm by manually measuring the microfibrils. Also on this fiber the MFA of 75° indicates that the measured cell wall is the S1 layer.

The 2 μm×2 μm AFM height image in figure 4.13a shows only few lignin precipitates. Due to an insufficient sample size (see figure 4.13b) a size distribution was not detectable. Thus, the mean value of the equivalent disc diameter of the lignin precipitates and its variation was here determined by calculating the average and the standard deviation, which led to 39 nm±13 nm. This high resolution image (figure 4.13a) shows a more open microfibril structure than the other 2 μm×2 μm AFM images on spruce fibers. The microfibril diameter on the top layer is 134 nm±26 nm, while the diameter of the microfibrils underneath is 65 nm±11 nm. This difference in microfibril width might come from a tip effect.

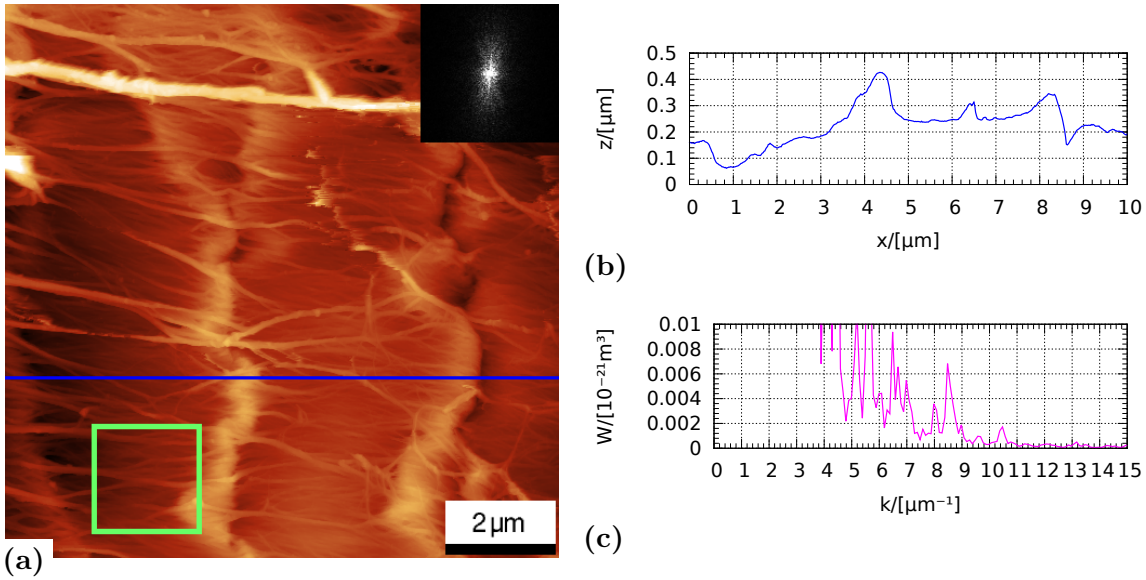

Figure 4.12: 10 μm×10 μm AFM height image of an 120 °C temperature treated spruce fiber, measured in water. (a) Height image, z-scale: 700 nm. The green square marks the position of the 2 μm×2 μm image in figure 4.13. The inset represents the 2D PSD of the AFM height image. (b) Line profile, the position is indicated by the blue line in (a). (c) PSD section at 85° with respect to the k_x-axis.

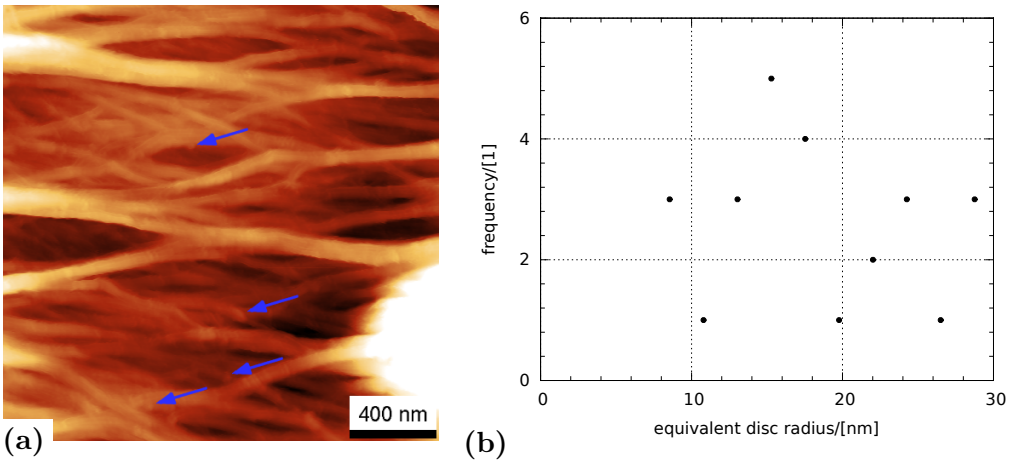

Figure 4.13: Lignin precipitates on an 120 °C treated spruce fiber. (a) 2 μm×2 μm height image, z-scale: 300 nm. The blue arrows indicate the position of lignin precipitates. (b) Size distribution of the lignin precipitates.

Summary

From the measured images it was possible to determine surface roughness σ, microfibril diameter, and the MFA of the investigated samples in the wet state. It could also be seen that the underlying curvature of the fiber surface influences the value of σ. This is, however, not desirable for this study, because the curvature of the fiber depends on the

position where the image was measured and conceals the roughness of wrinkles and fine structure. For this reason, all images were leveled by subtracting a third order polynom in x-direction and evaluated again, this time using HHCF for a comprehensive surface roughness characterization. Before flattening the mean value of σ for the $10\,\mu\text{m}\times10\,\mu\text{m}$ images of all four samples is $82\,\text{nm}\pm24\,\text{nm}$ and after flattening $69\,\text{nm}\pm11\,\text{nm}$, which means that the average value of the RMS roughness decreased but also the deviation, indicating that the roughness values of the investigated regions became more similar to each other. Table 4.2 summarizes the values calculated from the spruce fibers discussed so far.

Table 4.2: Summary of determined characteristics of the discussed $10\,\mu\text{m}\times10\,\mu\text{m}$ spruce fiber AFM height images. The values are always calculated from one AFM height image.

Sample	σ [nm]	$\sigma_{flatt.}$ [nm]	ξ [nm]	α [1]	MFA [°]	fibril size [nm]	precipitate size [nm]
23 ℃ (untr.)	70	66	867	0.70	78	$125\,\text{nm}^{+14\,\text{nm}}_{-11\,\text{nm}}$	$47\,\text{nm}\pm17\,\text{nm}$
80 ℃	109	73	646	0.60	66	$110\,\text{nm}^{+3\,\text{nm}}_{-3\,\text{nm}}$	$24\,\text{nm}\pm10\,\text{nm}$
100 ℃	56	54	477	0.85	80	$137\,\text{nm}^{+74\,\text{nm}}_{-36\,\text{nm}}$	-
120 ℃	93	81	725	0.60	75	$118\,\text{nm}^{+8\,\text{nm}}_{-7\,\text{nm}}$	$(39\,\text{nm}\pm13\,\text{nm})$*

*) Determined differently than the other values in this column (see text).

Beside $\sigma_{flatt.}$, also ξ and α have been calculated from the flattened $10\,\mu\text{m}\times10\,\mu\text{m}$ images. The values of the correlation parameter ξ are comparable to the width of the wrinkles on the surfaces and range from 477 nm to 867 nm, decreasing slightly with treatment temperature. The Hurst parameter α shows no trend and adopts values between 0.61 and 0.85.

The MFA ranges from 66° to 80°, which means, that the microfibrils are winding in a very flat left-handed helix around the fiber. This high MFA as well as the left-handed helix is expected from the S1 layer, although the helix could also be right-handed in the S1 layer. By taking only the MFA and the left- or right-handedness in account, the investigated layer could also be the S3 layer, but this is most unlikely, considering the fairly standard treatment of the pulp. If the S3 layer was at the surface, it would mean that the S1 and S2 layer had been removed and the S2 layer is the thickest of all [15].

The microfibril diameter was determined to be in the range of 110 nm to 137 nm, is higher than the values obtained in a dry state, where the diameter of the microfibrils is about 40 nm [37], and is not affected by temperature treatment.

Lignin precipitates were seen on the untreated, the 80 ℃ and the 120 ℃ temperature treated samples. The diameter of the lignin precipitates decreases from the untreated to the 80 ℃ treated sample but increases again on the 120 ℃ treated sample. With increasing treatment temperature, the number of grains are 165, 107, 0 and 26 and their relative projected surface areas are 8.34%, 1.72%, 0% and 0.86% respectively. The amount of lignin decreases with treatment temperature.

4.1.3 Pine

Untreated pulp

An AFM image of an untreated pine fiber surface measured in water is shown in figure 4.14. It is clearly visible that the microfibrils are randomly oriented, which is in contrast to all of the measured spruce samples. This lack of a preferred orientation indicates that the exposed layer is more likely the P layer.

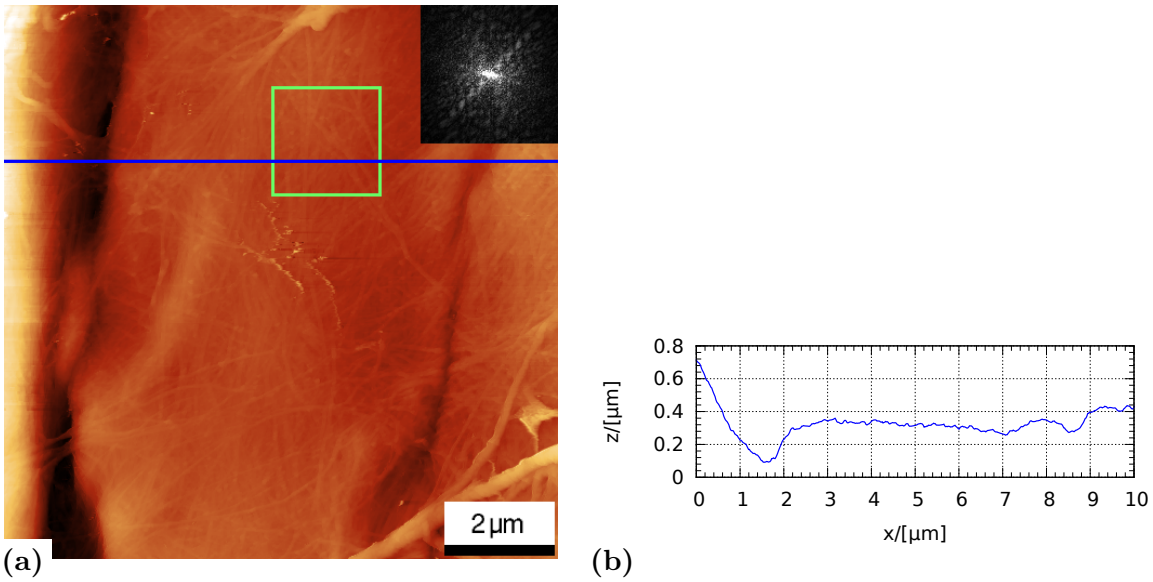

(a) (b)

Figure 4.14: 10 μm×10 μm AFM height image of an untreated pine fiber, measured in water. (a) Height image, z-scale: 800 nm. The green square marks the position of the 2 μm×2 μm image in figure 4.15. The inset represents the 2D PSD of the AFM height image. (b) Line profile, the position is indicated by the blue line in the height image.

Because the microfibrils are not oriented, and therefore not periodically aligned, it is not possible to calculate the microfibril size using PSD analysis. The only method to calculate the microfibril width is to manually measure microfibrils on different positions and averaging the values. All mean values of microfibril widths presented here, were averaged over 10 single measurements. This procedure gives a microfibril diameter of 120 nm±17 nm, which is comparable to the values obtained from the measured spruce fibers. Again surface wrinkles parallel to the main fiber axis occur, forming two trenches on the surface (approximately 300 nm and 90 nm deep). The RMS roughness of the AFM height image is 93 nm.

In the 2 μm×2 μm high-resolution AFM height image in figure 4.15a, lignin precipitates are visible on the microfibrils. The distribution of the lignin precipitate size is presented in figure 4.15b, indicating a precipitate diameter of 58 nm±29 nm. This value is higher than the one obtained from the untreated spruce sample.

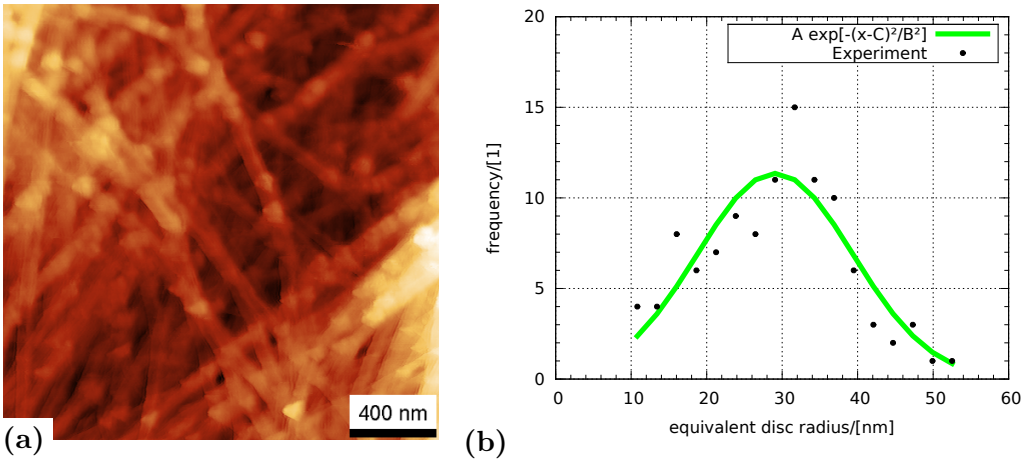

(a) (b)

Figure 4.15: Lignin precipitates on an untreated pine fiber. (a) $2\,\mu m \times 2\,\mu m$ height image, z-scale: 100 nm. (b) Size distribution of the lignin precipitates. The black dots are the data points determined from the experiment and the green line is a Gaussian fit.

Temperature treated pulp (80°C)

In figure 4.16, an AFM height image of an 80 ℃ temperature treated pine fiber, measured in water, is displayed. In contrast to the AFM image in figure 4.14, here a slight ordering of the microfibrils is observed, but not to such an extend as on the spruce samples.

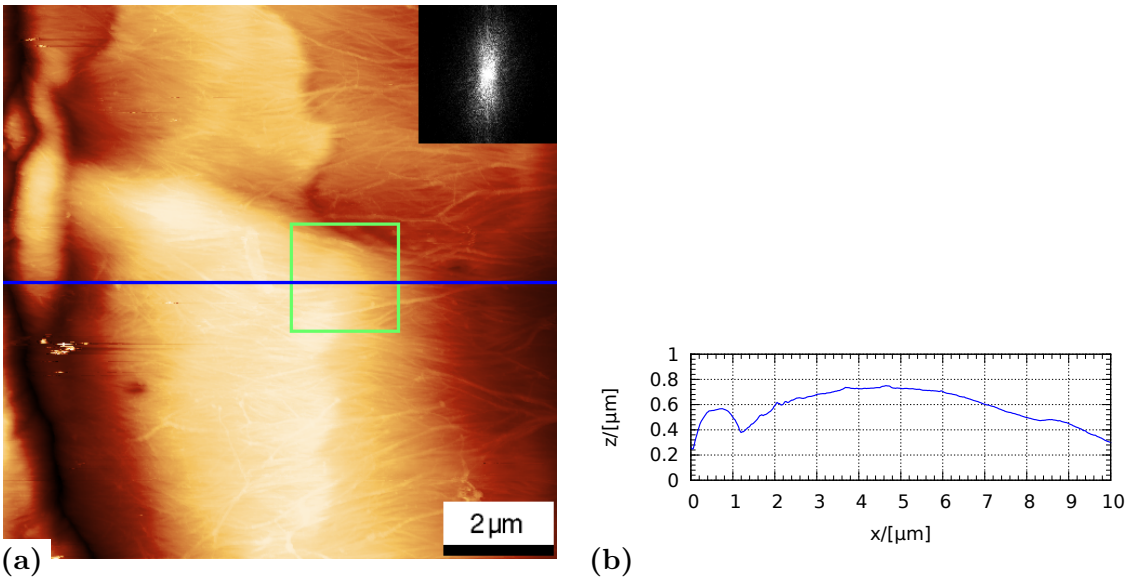

(a) (b)

Figure 4.16: $10\,\mu m \times 10\,\mu m$ AFM height image of an 80 ℃ temperature treated pine fiber, measured in water. (a) Height image, z-scale: 1000 nm. The green square marks the position of the $2\,\mu m \times 2\,\mu m$ image in figure 4.17. The inset represents the 2D PSD of the AFM height image. (b) Line profile, the position is indicated by the blue line in the height image.

The 2D PSD slightly shows microfibrils with two preferred orientations and hence two MFA values of 65° and 105°. Because of that, the measured surface area can be still in the P layer, the transition region from P to S1, or in the S1 layer. The surface is smooth and curved with a RMS roughness of 118 nm and showing wrinkles on the far left side and the center of the image. A manual evaluation leads to a fibril width of 130 nm±45 nm.

In the high resolved AFM image in figure 4.17a, less lignin precipitates than on the untreated pine fiber surface is observable. They are also smaller in diameter, which is represented by an average precipitation diameter of 32 nm±15 nm (see figure 4.17b). The lignin precipitates are always found on the microfibrils and not between them. The microfibrils are on this scale well oriented and they form a dense packed structure.

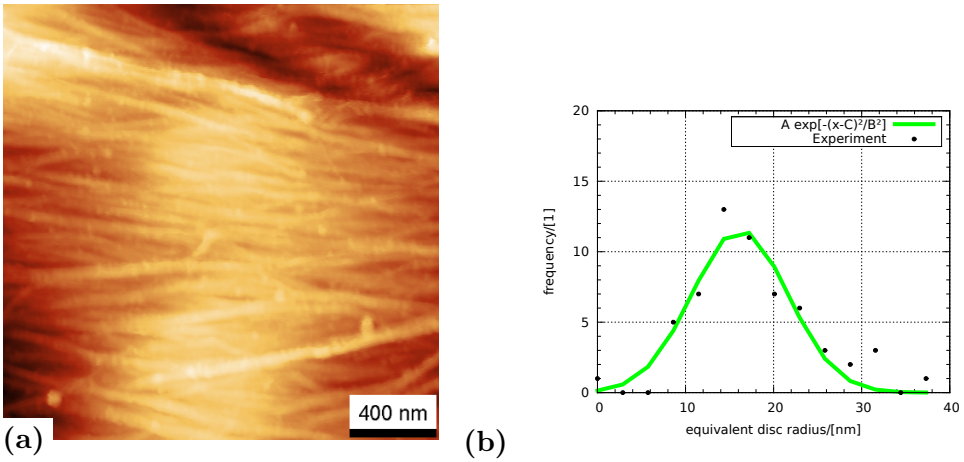

(a) (b)

Figure 4.17: Lignin precipitates on an 80 °C temperature treated pine fiber. (a) 2 μm×2 μm height image, z-scale: 150 nm. (b) Size distribution of the lignin precipitates. The black dots are the data points determined from the experiment and the green line is a Gaussian fit.

Temperature treated pulp (100°C)

The AFM image of the 100°C temperature treated pine fiber in figure 4.18 measured in water is presented. It shows a curved surfaces with mostly randomly oriented microfibrils. Only in the upper part, above the large horizontally oriented microfibril bundle, the microfibrils are ordered. In spite of the slight ordering in the upper part of the image, it is still most likely that the P layer is the measured cell wall layer. The manually determined microfibril width amounts to 143 nm±48 nm, which is a value at the higher end of the microfibril width range obtained for the other samples. Caused by the curved surface, the RMS roughness of 126 nm is rather high in comparison to the other measurements.

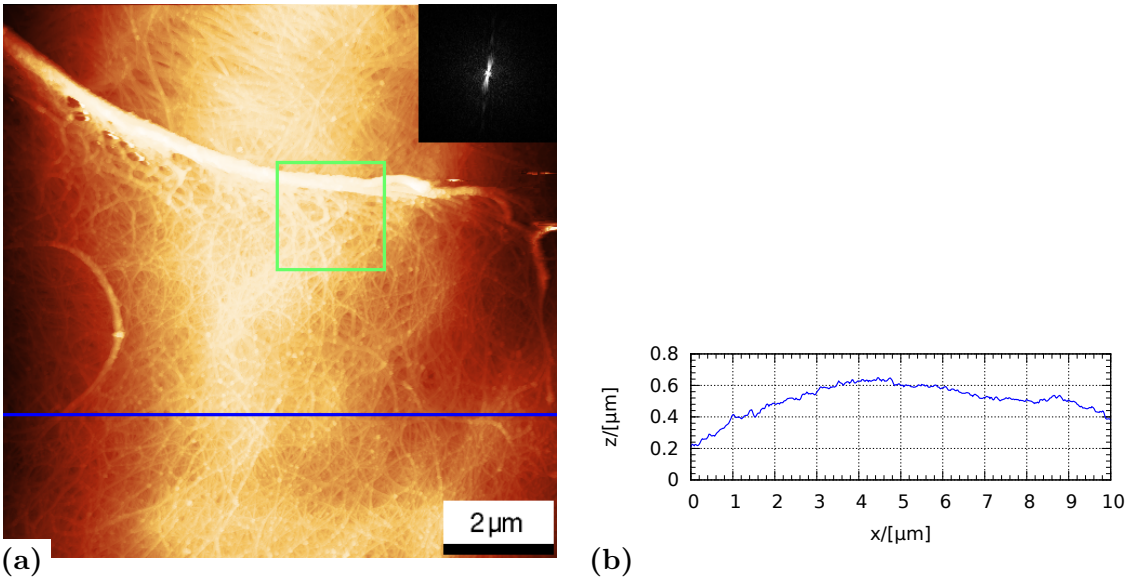

(a) (b)

Figure 4.18: 10 μm×10 μm AFM height image of an 100 °C temperature treated pine fiber, measured in water. (a) Height image, z-scale: 900 nm. The green square marks the position of the 2 μm×2 μm image in figure 4.19. The inset represents the 2D PSD of the AFM height image. (b) Line profile, the position is indicated by the blue line in the height image.

In figure 4.19a the microfibrils are randomly oriented, forming a structure comparable to the untreated sample.

Lignin precipitates are again visible on the microfibrils, with a size of 61 nm±26 nm and their distribution is presented in figure 4.19b. This precipitate size is comparable to the precipitate size on the untreated sample. A fibril bundle, formed by two or possibly three microfibrils, is observable in the upper part of the AFM height image.

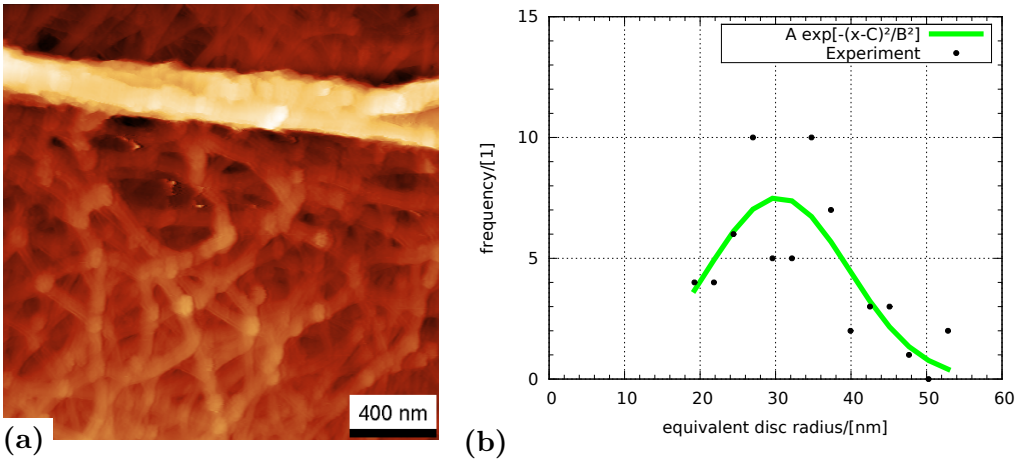

Figure 4.19: Lignin precipitates on an 100 ℃ temperature treated pine fiber. (a) 2 μm×2 μm height image, z-scale: 250 nm. (b) Size distribution of the lignin precipitates. The black dots are the data points determined from the experiment and the green line is a Gaussian fit.

Temperature treated pulp (120°C)

As can be seen from the AFM image in figure 4.20 that this 120 ℃ treated fiber surface looks similar to that of the 100 ℃ treated one. No preferred microfibril orientation is visible, leading again to the conclusion that the P layer was measured. Also, some fibril bundles are observed on the left side of the scanned region. The surface is strongly curved in the horizontal direction, resulting in an RMS roughness of 531 nm, which is very high compared to the images taken on the other pine or spruce fibers. The manually determined microfibril diameter of 116 nm±26 nm compares very well to the values from the other samples.

Figure 4.21 represents another fiber surface of the same treated pulp which is similar to the one of the 80 ℃ temperature treated pulp fiber (figure 4.16). Here, a potential orientation is slightly present but it is not as defined as observed on the spruce fibers. Both, the AFM image and the FFT of the image, show that the microfibrils are oriented but with two distinct values of the MFA, which are 75° and 110°. Therefore, the measured surface region could be already in the S1 layer, in the P layer or in the transition region between P and S1 layer. From the line profile, it can be seen that on the left side of the AFM image a curvature is present, which transforms into a plateau that represents the largest part of the image. An RMS roughness of 164 nm is calculated, which is still very high and is comparable to the AFM height image in figure 4.20a. The manual evaluation yields a fibril width of 108 nm±22 nm, which is the lowest value observed on the wet fiber samples. On the very left side of the AFM height image in figure 4.21 knots – lined up on the edge – are visible, which are possibly agglomerated microfibrils.

The microfibrils on the 120 ℃ temperature treated pine fiber (see figure 4.22a) are dense packed, and a high amount of lignin precipitates (13.7% of the scanned area of

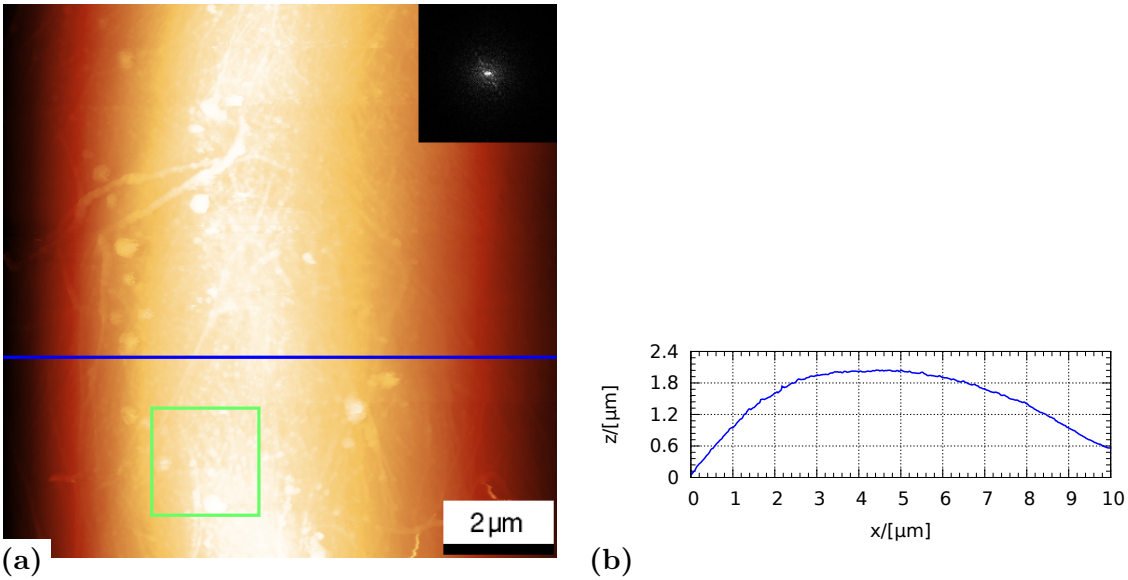

(a) (b)

Figure 4.20: 10 μm×10 μm AFM image of an 120℃ temperature treated pine fiber, measured in water. (a) Height image, z-scale: 2200 nm. The green square marks the position of the 2 μm×2 μm image in figure 4.22. The inset represents the 2D PSD of the AFM height image. (b) Line profile, the position is indicated by the blue line in the height image.

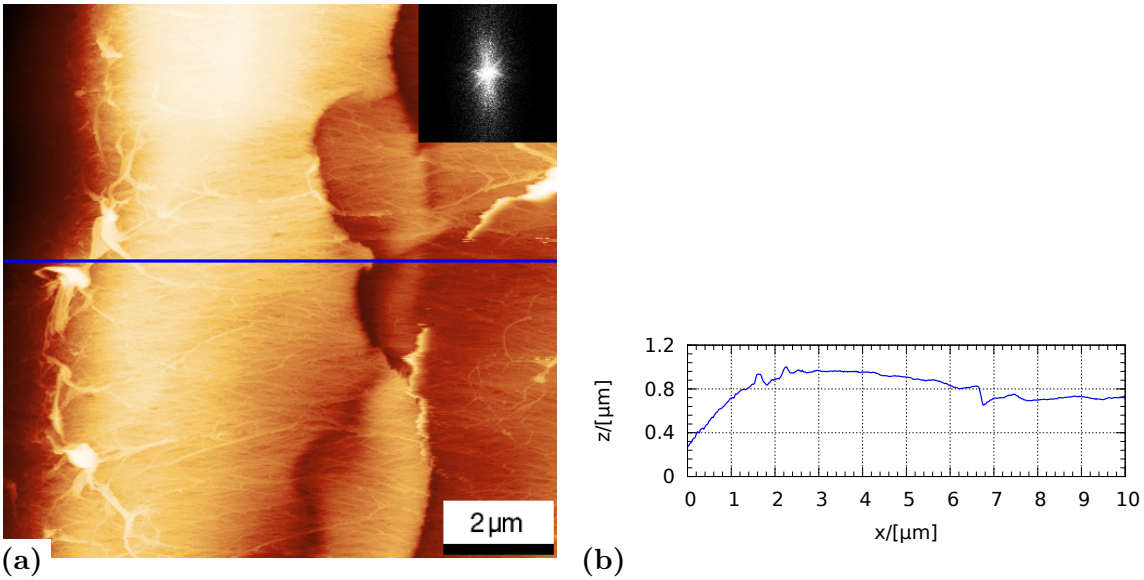

(a) (b)

Figure 4.21: 10 μm×10 μm AFM height image of an 120 ℃ temperature treated pine fiber, measured in water. (a) Height image, z-scale: 1300 nm. The inset represents the 2D PSD of the AFM height image. (b) Line profile, the position is indicated by the blue line in (a).

4 μm^2) is visible. The size of the precipitates is 56 nm±24 nm and is comparable to the precipitate sizes of the untreated and the 120 ℃ treated sample. The lignin precipitates are again found always on the microfibrils.

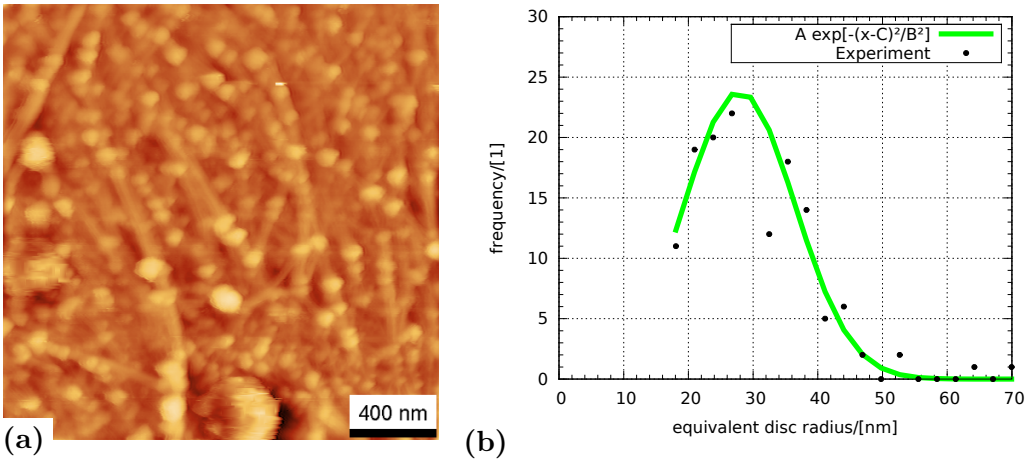

Figure 4.22: Lignin precipitates on an 120 ℃ temperature treated pine fiber. (a) 2 μm×2 μm height image, z-scale: 150 nm. (b) Size distribution of the lignin precipitates. The black dots are the data points determined from the experiment and the green line is a Gaussian fit.

Summary

From the pine fiber samples in water, σ, microfibril diameter, and the lignin precipitate size distribution could be obtained. Due to a lack of preferred orientation of the microfibrils it was not always possible to determine an MFA. The RMS roughness, measured from the unflattened AFM height images discussed so far, increased with increasing treatment temperature. This was due to a high curvature of the measured region, as a flattening with a third order polynom in x-direction reduces the roughness values significantly. The average roughness value changes from 217 nm±210 nm before flattening to 67 nm±19 nm after flattening. More similar roughness values are obtained after flattening, which is indicated by a smaller standard deviation. Also, a roughness characterization with the parameters ξ and α additional to the RMS roughness was performed on the flattened images. Table 4.3 summarizes the extracted values from the pine fiber samples.

Table 4.3: Summary of determined characteristics of the discussed 10 μm×10 μm pine fiber AFM height images. The values are always calculated from one AFM height image.

Sample	σ [nm]	$\sigma_{flatt.}$ [nm]	ξ [nm]	α	MFA [°]	fibril size [nm]	precipitate size [nm]
23 ℃ (untr.)	93	89	490	0.80	-	120 nm±17 nm	58 nm±29 nm
80 ℃	118	78	690	0.65	64–104	130 nm±45 nm	32 nm±15 nm
100 ℃	126	51	830	0.55	-	143 nm±48 nm	61 nm±26 nm
120 ℃	531	51	1080	0.60	(74–108)*	116 nm±27 nm	56 nm±24 nm

*) Determined from a different image than the other values.

The surface roughness after flattening $\sigma_{flatt.}$ shows a decrease of the roughness with increased temperature. This could be interpreted as an increase of the width of surface wrinkles. The Hurst parameter α seems to have no relation with treatment temperature.

An MFA could only be determined from two AFM height images, where the MFA did not assume a single value and suggests crossed microfibrils. This could be interpreted in several ways: First, the surface layer is part of the P layer, but the slight orientation could also indicate that, second, the surface is part of the S1 layer or, third, at the transition region from P to S1. Most of the measured regions showed only randomly oriented microfibrils, which leads to the conclusion that the exposed layer is the P layer.

The average microfibril diameter assumes values between 120 nm and 143 nm and seems to be independent of treatment temperature. The values are comparable to those of the spruce fibers and therefore also higher than the microfibril widths determined in the dry state (about 40 nm) [37].

All investigated regions showed lignin precipitates on the microfibrils. The average lignin precipitate diameter is always around 60 nm, except for the region measured on the 80 ℃, where the mean diameter of the precipitates was 32 nm±15 nm. The numbers of lignin precipitates on the scanned areas of 4 μm^2 are with increasing treatment temperature 109, 59, 62 and 164 with a coverage of 8.42%, 1.95%, 5.71% and 13.71% respectively. Here, the amount of lignin is first decreasing then rising again to a value higher than the one obtained from the untreated sample.

4.1.4 Comparison of spruce and pine fibers

Surfaces of spruce and pine fibers have been investigated in the wet state. The most obvious difference between spruce and pine fibers is the outer cell wall. For spruce, without exception, always the S1 layer was the exposed one, whereas for pine mostly the P layer, the S1 layer, or the transition region between S1 and P was the one investigated by AFM.

Figure 4.23 compares the microfibril diameters obtained from spruce fibers with those of pine fibers. For both pulps the microfibril diameter does not change significantly with treatment temperature. Also there is no significant difference between spruce and pine.

Spruce fibers have an average surface roughness of 81 nm±27 nm, which is lower than the average surface roughness of the pine fibers of 93 nm±44 nm. These values are the average values from all AFM scans after flattening with a 3rd order polynom for every treatment temperature. The average roughness values of the spruce fibers are calculated from 12 10 μm×10 μm scans and the roughness values of the pine fiber surfaces from 11 10 μm×10 μm scans. Figure 4.24 displays these roughness values over treatment temperature and visualizes also the effect of the third order flattening of the AFM images (see figures 4.24c and 4.24d). The roughness values obtained from pine fibers were more affected by flattening, because their surfaces were more curved than those of the spruce fibers.

From every pulp sample at least two 10 μm×10 μm images were recorded. This allowed to calculate average surface roughness values for each treatment temperature.

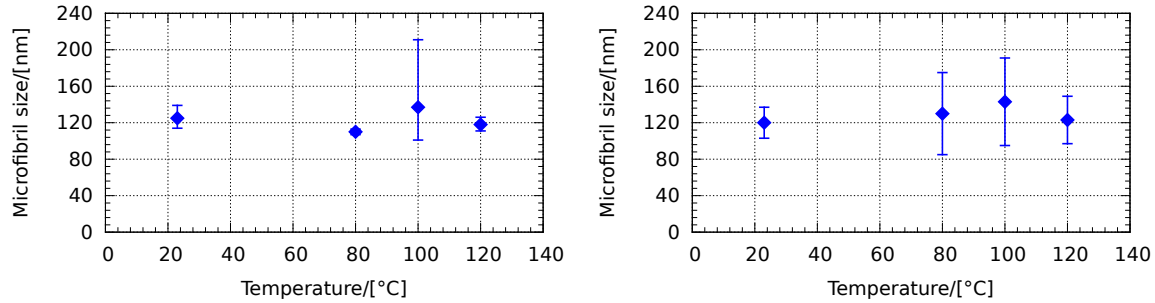

(a) (b)

Figure 4.23: Microfibril size over temperature for (a) spruce (determined from PSD) and (b) pine (manually measured).

Figures 4.24a and 4.24b present the averaged roughness values over treatment temperature, all values obtained from third order flattened AFM height images. Considering the error bars, there is no significant change of σ with treatment temperature and also the roughness values between spruce and pine seem not to differ significantly.

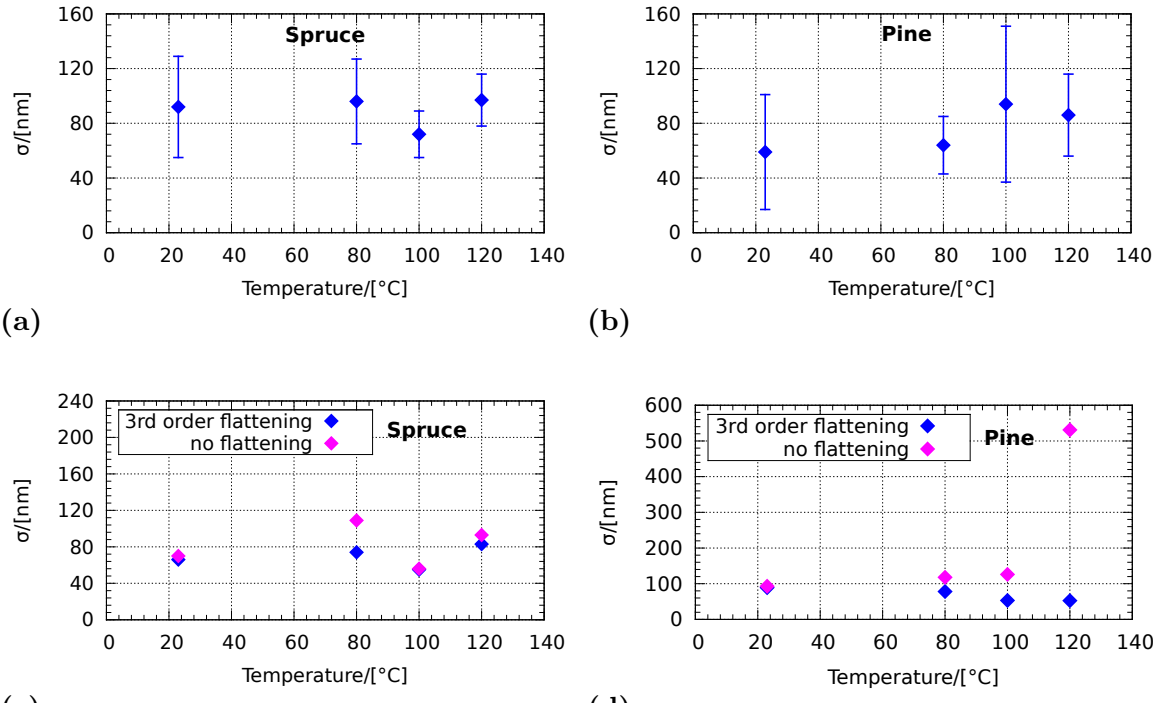

(a) (b)

(c) (d)

Figure 4.24: RMS roughness values over temperature, determined from 10 μm×10 μm. Average σ of (a) spruce and (b) pine surfaces, all with third order flattening and averaged over two images, except spruce 80 ℃ (four), 100 ℃ (three) and pine 120 ℃ (three).(c) Spruce and (d) pine before and after flattening with a third order polynom.

In figures 4.25a and 4.25b, the equivalent disc diameter of precipitated lignin parti-

cles on the measured pulp fiber surfaces is presented as a function of fiber treatment temperature. The spruce samples show a slight decrease in precipitate diameter with increasing treatment temperature, whereas the pine samples show a constant lignin precipitate diameter of about 60 nm. Only for the 80 °C temperature treated pine sample a smaller value compared to the other scans on the pine fiber surfaces was observed.

The relative surface area coverage of the lignin precipitates is displayed in figures 4.25c and 4.25d for spruce and pine respectively. On the scanned regions of the spruce fiber surfaces, the lignin coverage is decreasing with increasing treatment temperature. The scanned pine fiber surface regions show first a decrease of coverage followed by an increase to a coverage higher than obtained from the untreated sample. For an individual temperature, the coverage is on a pine fiber surface always higher than on a spruce fiber surface. This can be explained by the different outer cell wall layers. In the P layer more lignin is found than in the S1 layer. Therefore, a higher lignin coverage is found on the pine fiber samples, where the P layer represents the outer layer. The increase of lignin coverage at higher treatment temperatures could be explained by a reprecipitation of the already dissolved lignin.

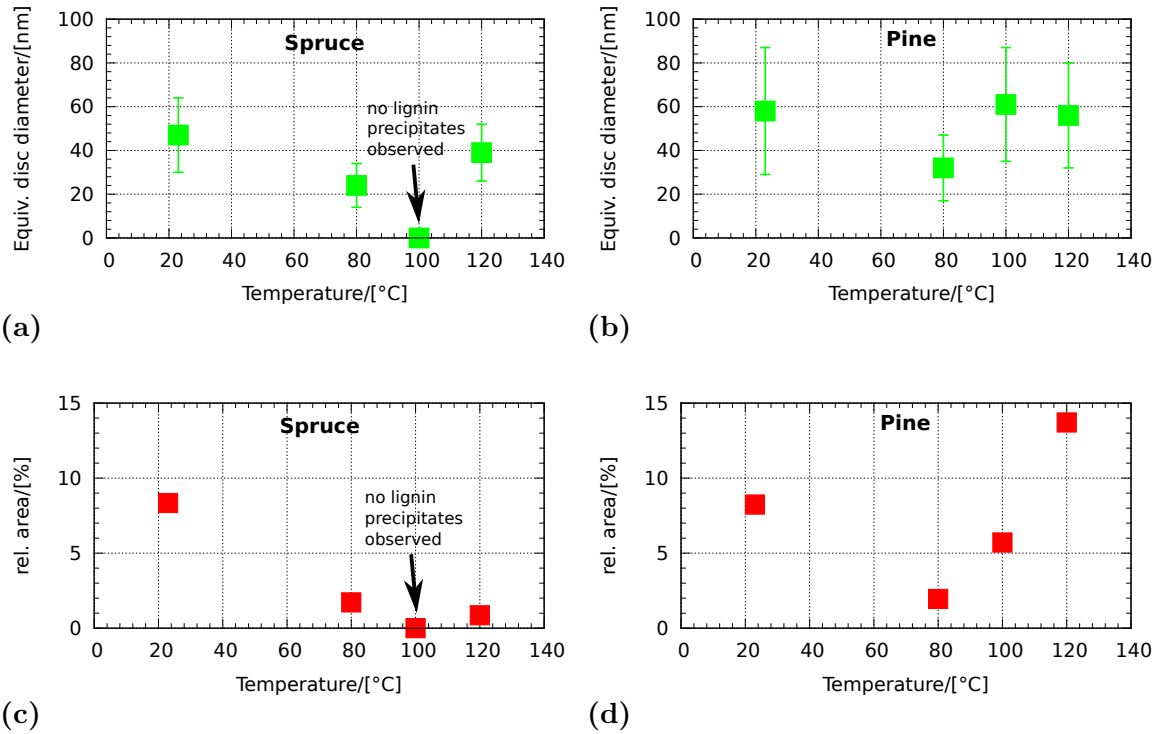

Figure 4.25: Quantification of lignin precipitates on pulp fibers. Average equivalent disc diameter of lignin precipitates on (a) spruce and (b) pine fiber surfaces over temperature. Relative surface area coverage of lignin precipitates on (c) spruce and (d) pine fiber surfaces over temperature.

4.2 Surface morphology of regenerated cellulose fibers

In contrast to the measurements on the pulp fiber surfaces, the regenerated cellulose fibers were investigated only in the dry state. The sample preparation and setup for the measurements on regenerated fiber surfaces is explained in detail in sections 3.2 and 3.3.

4.2.1 Bellini 1

Bellini 1 fibers are hollow and collapsed viscose fibers, showing a low breaking length and a high number of double folds, when formed into a sheet. Figure 4.26 represents a 20 μm×20 μm AFM image of a Bellini 1 fiber surface. The surface is very smooth with only a slight curvature. Wrinkles with a size of about 500 nm can be observed.

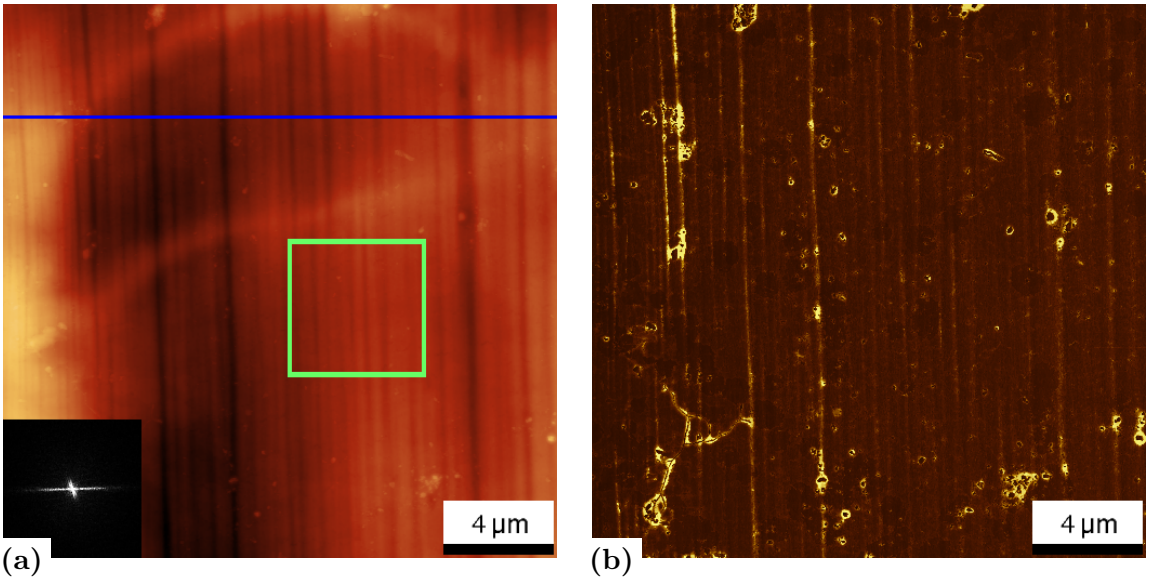

(a) (b)

Figure 4.26: 20 μm×20 μm image of a Bellini 1 fiber surface. (a) Height image, z-scale: 600 nm, the blue line marks the position of the line profile in figure 4.27a and the green square marks the zoom-in, presented in figure 4.28a. The inset represents the 2D PSD of the AFM height image. (b) Phase image, z-scale: 90°.

To evaluate characteristic sizes of the surface, a line profile and the PSD have been analyzed, both are displayed in figure 4.27. First the wrinkle size is calculated manually from the line profile in figure 4.27a by measuring the distances between to neighboring valleys. This was done over the entire profile, giving the mean value and the standard deviation of the wrinkle size. The manually calculated wrinkle size is 529 nm±206 nm. The PSD section in figure 4.27b shows several peaks but the comparison with the average size from the line profile suggests that the peaks corresponding to $495\,\mathrm{nm}^{+11\,\mathrm{nm}}_{-11\,\mathrm{nm}}$ and $625\,\mathrm{nm}^{+18\,\mathrm{nm}}_{-17\,\mathrm{nm}}$ in real space are describing the surface wrinkles best.

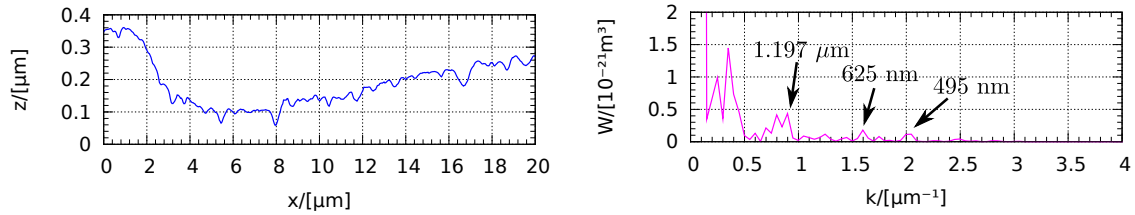

Figure 4.27: Bellini 1, evaluation. (a) Line profile from 20 μm×20 μm image, the position is marked by the blue line in figure 4.26. (b) Section of the 2D PSD (see inset in figure 4.26a) at an angle of 1° with respect to the k_x-axis.

By decreasing the scan range to 5 μm×5 μm (figure 4.28), the surface wrinkles are higher resolved and also finer structures are starting to be vaguely visible. The manual evaluation of the line profile in 4.27a gives a wrinkle size of 566 nm±167 nm and the PSD analysis a size of 575 nm$^{+221\,\mathrm{nm}}_{-125\,\mathrm{nm}}$. Both values correspond well to the sizes calculated from the 20 μm×20 μm image. The values differ because the 5 μm×5 μm is only a sixteenth of the larger image and providing therefore less statistics for the determination of the wrinkle size. It is also visible that the wrinkles on the left side of the 20 μm×20 μm image in figure 4.26a are smaller compared to the wrinkles on the right side, where the 5 μm×5 μm is taken, and therefore explaining the higher values.

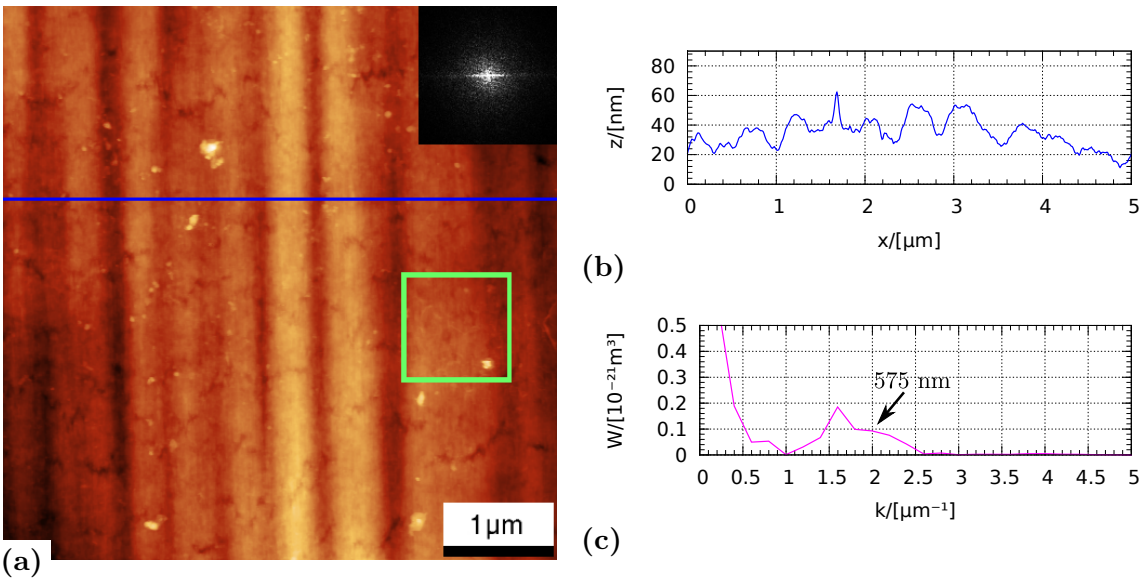

Figure 4.28: Bellini 1, 5 μm×5 μm zoom. (a) Height image, z-scale: 90 nm, the green square marks the zoom-in, shown in figure 4.29. The inset represents the 2D PSD of the AFM height image. (b) Line profile at the position marked by the blue line in (a). (c) Section of the 2D PSD at an angle of 1° with respect to the k_x-axis.

To look for features with a size below 100 nm, the scan size was reduced further to

$1\,\mu\text{m}\times1\,\mu\text{m}$. In figure 4.29 small fibrils become visible in topography. In the phase image the contrast is even enhanced revealing the fine structure of the fiber surface best. Therefore, the line section as well as the PSD spectrum were both extracted from the phase image. It can be seen that most fibrils are oriented almost parallel to the fiber axis, but some of them are aligned perpendicular to the main orientation. Manual evaluation results in a fibril size of $29\,\text{nm}\pm12\,\text{nm}$ and the PSD analysis gives a size of $30\,\text{nm}^{+2\,\text{nm}}_{-2\,\text{nm}}$.

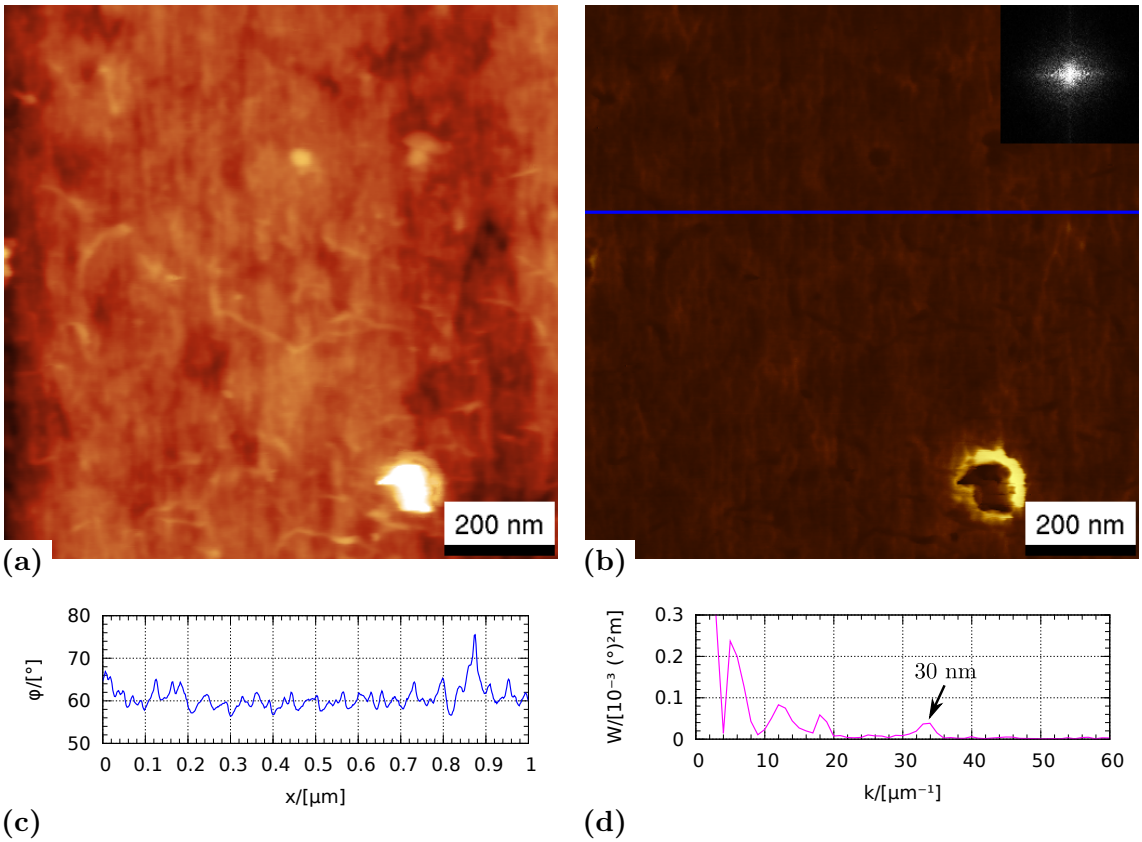

Figure 4.29: Bellini 1 $1\,\mu\text{m}\times1\,\mu\text{m}$ zoom. (a) Height image, z-scale: 40 nm. (b) Phase image, z-scale: 90°. The inset represents the 2D PSD of the AFM height image. (c) Line profile at the position marked by the blue line in the phase image. (d) PSD section at an angle of 1° with respect to the k_x-axis.

To calculate the MFA, the tilt of the fiber with respect to the vertical axis was measured from the optical image, and the angle of the fibrils to the AFM images vertical axis was extracted from the 2D FFT (see sections 2.4 and 3.3 for details). The MFA for Bellini 1 is then 0.2° and the angle of the surface wrinkles with respect to the main fiber axis, calculated the same way, is 0.1°. Both values, the MFA and the angle of wrinkles to the main fiber axis, suggest that the orientation of the respective features is approximately parallel to the main fiber axis.

4.2.2 Bellini 4

Bellini 4 fibers are of the same type as Bellini 1 fibers, but when formed into a sheet they show a high breaking length and a low number of double folds, which is opposite to Bellini 1. The 20 μm×20 μm AFM height image in figure 4.30 shows again a smooth surface but with a 2 μm wide and 200 nm deep trench, approximately parallel to the fiber axis. Surface wrinkles can be seen again, but they are less pronounced than in the Bellini 1 image (figure 4.26). A manual evaluation of the line section in figure 4.30b results in a surface wrinkle size of 778 nm±284 nm. The PSD section in figure 4.30c reveals two peaks corresponding to sizes of $719\,\mathrm{nm}^{+45\,\mathrm{nm}}_{-40\,\mathrm{nm}}$ and $1007\,\mathrm{nm}^{+121\,\mathrm{nm}}_{-97\,\mathrm{nm}}$. Both values obtained from the 2D PSD analysis are within the range of the manual calculation, while the manual calculated mean value is between the values obtained from PSD analysis, which suggests a bimodal distribution of surface wrinkles like in Bellini 1. A comparison with Bellini 1 shows that the wrinkles are larger on the Bellini 4 surface.

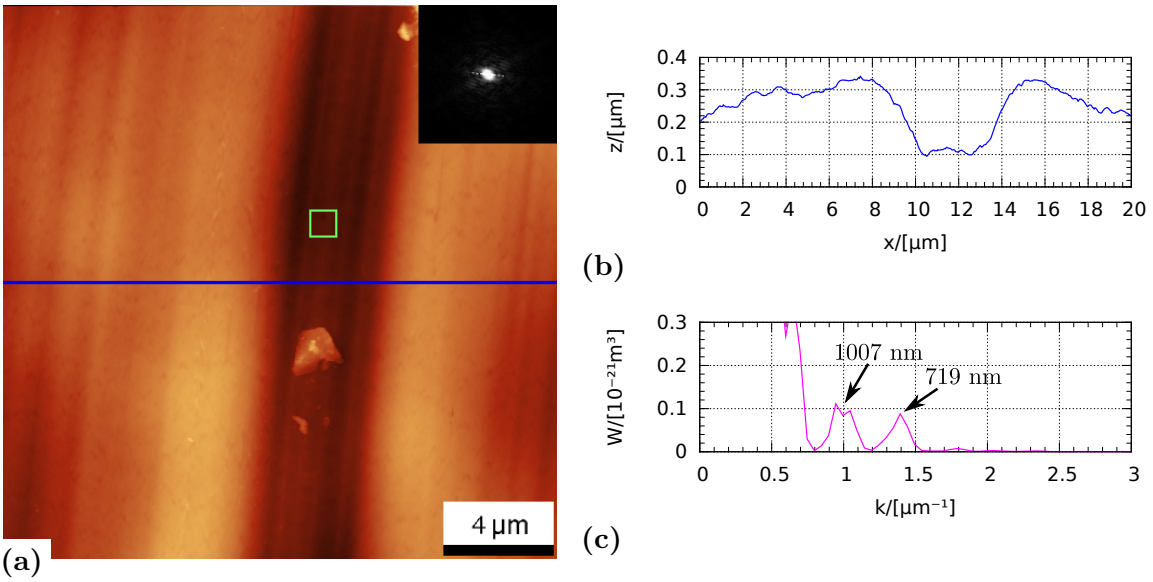

Figure 4.30: Bellini 4 20 μm×20 μm height image. (a) Height image, z-scale: 600 nm. The inset represents the 2D PSD of the AFM height image. (b) Line profile, the position is indicated by the blue line in the height image. (c) PSD section at -6° with respect to the k_x-axis.

Figure 4.31 shows a 1 μm×1 μm phase image of the Bellini 4 fiber surface, revealing again a fibrillar structure. The manual calculation gives a fibril size of 33 nm±12 nm and the evaluation of the PSD section yields a size of $38\,\mathrm{nm}^{+3\,\mathrm{nm}}_{-2\,\mathrm{nm}}$. Again, the phase image reveals an enhanced contrast compared to the height image on the lower scale and was therefore used to determine the fibril size. With the knowledge that the fiber is placed with its main axis perpendicular to the cantilevers fast scanning axis and that the trench – visible in figure 4.30 – is parallel to the fiber's main axis, the MFA was determined to be about 0°.

In figure 4.32, another AFM height image of the same Bellini 4 fiber, but recorded

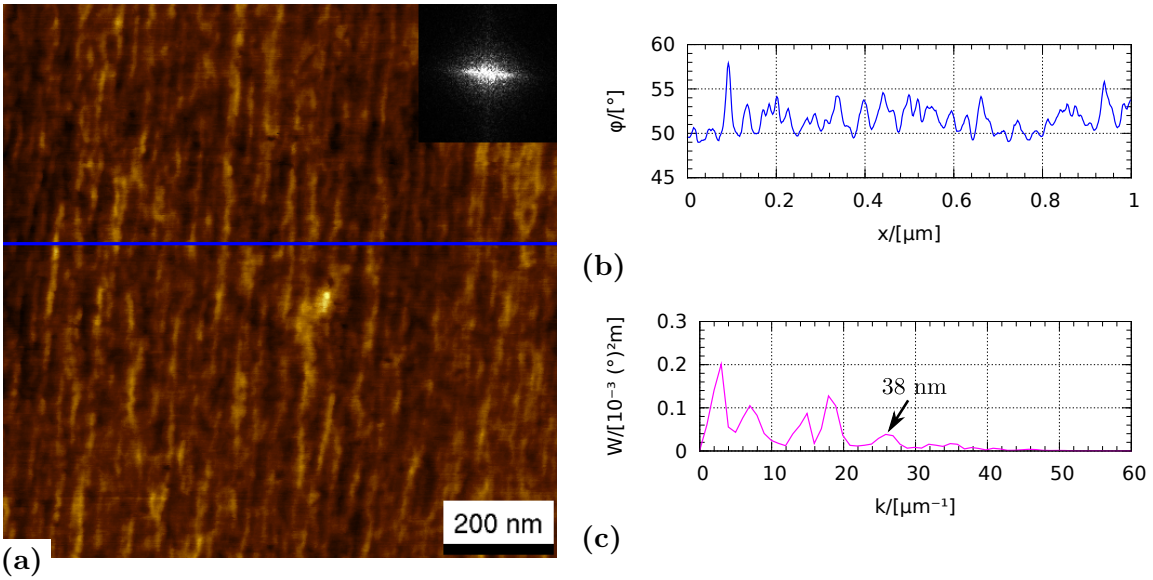

Figure 4.31: Bellini 4 1 μm×1 μm phase image, its position is indicated by the green square in figure 4.30a. (a) Phase image, z-scale: 15°. The inset represents the 2D PSD of the AFM height image. (b) Line profile along the blue line in the height image. (c) Cross-section of the 2D PSD taken at -6° with respect to the k_x-axis.

four months after the first measurement, is displayed. The surface in figure 4.32a shows a 600 nm deep trench parallel to the fiber axis and surface wrinkles, which are $901\,\mathrm{nm}^{+447\,\mathrm{nm}}_{-224\,\mathrm{nm}}$ wide. The angle of the wrinkles to the main fiber axis is 0°. The 1 μm×1 μm phase image in figure 4.32b shows again the fibrillar structure with a mean fibril width of $31\,\mathrm{nm}^{+6\,\mathrm{nm}}_{-4\,\mathrm{nm}}$ and an MFA of 0°. Compared to figure 4.30a, the surface in figure 4.32a looks similar with the vertical trench running through the image. Also the overall shape of the surface is comparable. But figure 4.32a shows contaminations which have not be seen in figure 4.30. These might be particles that were adsorbed during storage under ambient conditions, for four months.

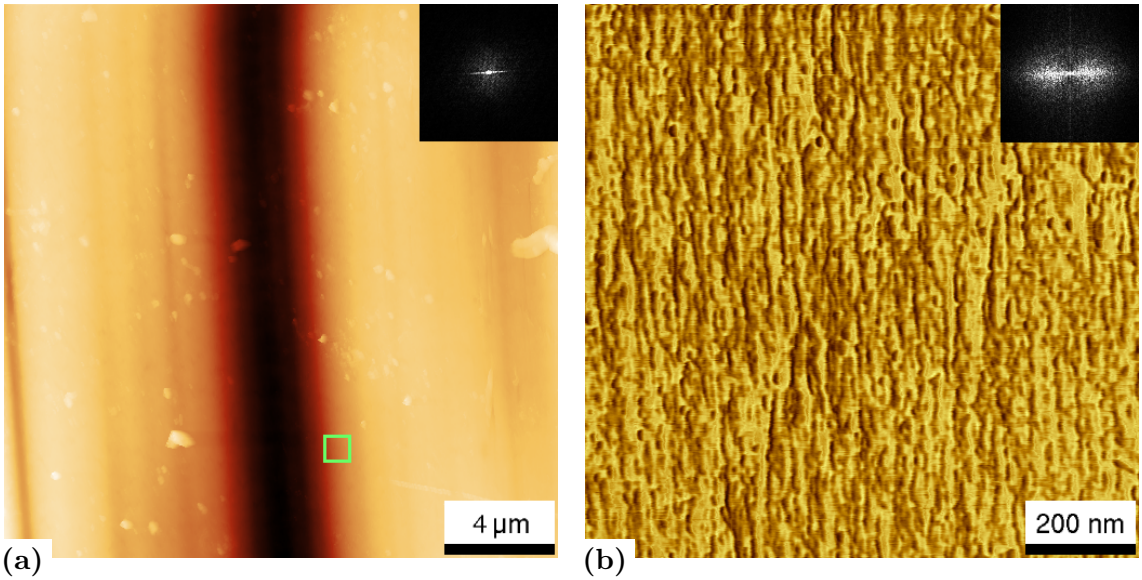

(a) (b)

Figure 4.32: Bellini 4 fiber surface. (a) 20 μm×20 μm, z-scale: 900 nm. (b) 1 μm×1 μm phase image, z-scale: 35°. Its position is marked by the green square in (a). The insets represent the 2D PSD of the AFM height image.

4.2.3 Cellini

Cellini fibers are Bellini 4 fibers where 5% CMC was added. As can be seen from figure 4.33, the surface is still smooth but covered with the added CMC. Like on the Bellini 4 surface, also here a trench – which is almost vertically oriented – is visible. This time it is narrower (about 200 nm at the bottom) while the depth is the same. On most parts of the surface, it is still possible to identify the wrinkles. The manual determination of their size results in 507 nm±174 nm and the evaluation of the PSD gives $587\,\mathrm{nm}^{+30\,\mathrm{nm}}_{-26\,\mathrm{nm}}$.

Using the watershed algorithm, it was possible to mark the regions which are covered with CMC. To successfully use the algorithm, it was necessary to flatten the image. The modification was carried out by applying polynomial flattening and FFT filtering to the image in figure 4.33a. The result of the flattening as well as the marked grains can be seen in figure 4.33b. The used polynom was of degree 3 in the horizontal direction and of degree 6 in the vertical direction. For FFT filtering, an elliptical region with major axis length of 1.3 $\mu\mathrm{m}^{-1}$, a minor axis length of 1.1 $\mu\mathrm{m}^{-1}$ and horizontally oriented was masked at the center of the 2D FFT. With this, the percentage of CMC on the surface was calculated to be 15% which is 3 times higher than the added CMC amount of 5%. Here, also higher resolved images were recorded, but due to the covering with CMC it was not possible to observe a fine structure on this surface. The reason is either because the CMC is covering the smaller features or the AFM tip had picked up some CMC making it impossible to resolve the fine structure.

Figure 4.34 presents the size distribution of the CMC agglomerates on the Cellini fiber surface. It is visible that the distribution has its maximum near the lowest observed

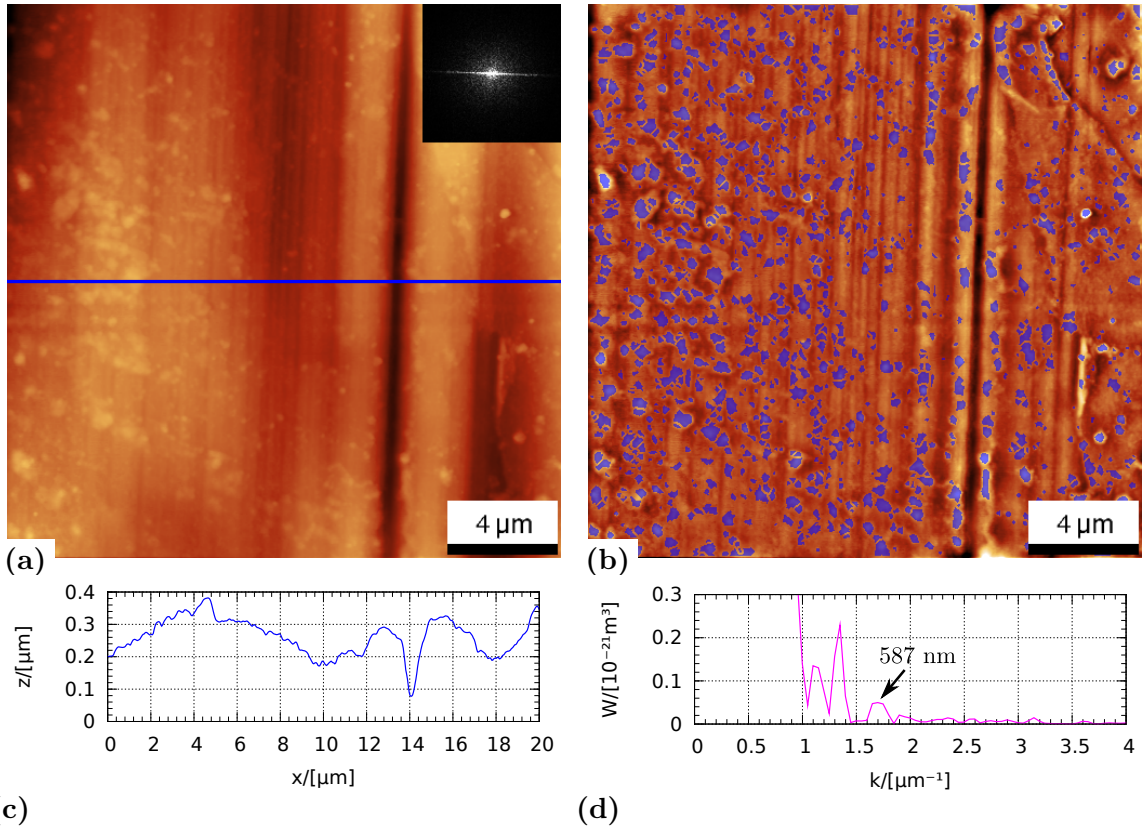

Figure 4.33: Cellini 20 μm×20 μm height image. (a) Height image, z-scale: 600 nm. The inset represents the 2D PSD of the AFM height image. (b) Height image, polynomial leveled and FFT filtered; the blue spots mark the CMC on the surface; z-scale: 150 nm. (c) Line profile at the position indicated by the blue line in the height image. (d) PSD section at -2° with respect to the k_x-axis.

CMC particle diameter. Therefore, the distribution of the particle radius r was fitted with a lognormal distribution (see equation 2.11), yielding a mean value of 61 nm and a deviation of 67 nm.

4.2.4 Classic viscose

Two types of classic viscose fibers were analyzed. One fiber was stretched by 5%, the other fiber by 40%. Due to the fact that the Bellini and Cellini fibers were collapsed, it was possible to scan 20 μm×20 μm areas since the surface was flat over large distances. For classic viscose, however, the largest possible image size was 10 μm×10 μm. Figure 4.35 shows the 10 μm×10 μm height images and extracted line profiles of the differently stretched fibers. Both images show a surface morphology corresponding to the cross-section presented in section 2.3 in figure 2.5a, which was expected from classic viscose fibers.

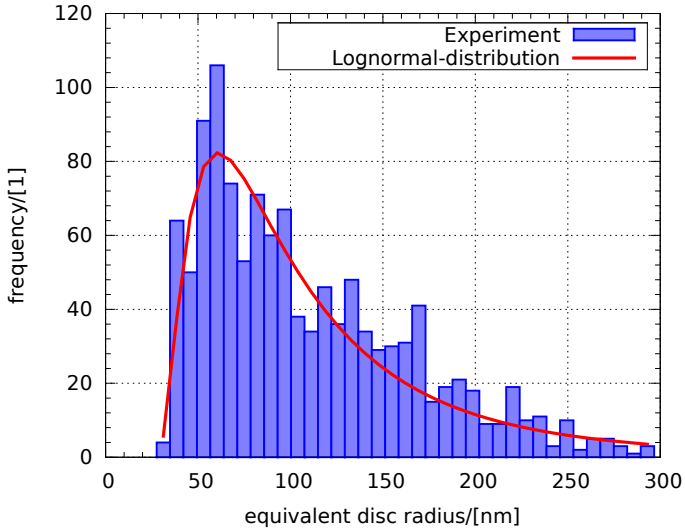

Figure 4.34: Size distribution of CMC on the viscose fiber surface fitted with a log-normal distribution (red line).

The manual and PSD evaluation of the wrinkle size gives for 5% stretched classic viscose 3197 nm±930 nm and 3212 $\mathrm{nm}^{+1992\,\mathrm{nm}}_{-889\,\mathrm{nm}}$ respectively and for 40% stretched classic viscose 3317 nm±78 nm and 3716 $\mathrm{nm}^{+2564\,\mathrm{nm}}_{-1078\,\mathrm{nm}}$. A comparison shows that the wrinkles are slightly larger for the 40% stretched classic viscose. The angle of the wrinkles to the main fiber axis is 1.1° for the 5% stretched classic viscose fiber and 2.1° for the 40% stretched classic viscose fiber.

In figure 4.36, 1 μm×1 μm phase images of the two classic viscose fiber types are displayed. Due to the enhanced contrast, the phase images were used for the evaluation and only these are presented here. For the 5% stretched classic viscose, the fibril size is 31 nm±10 nm from manual evaluation and 39 $\mathrm{nm}^{+4\,\mathrm{nm}}_{-2\,\mathrm{nm}}$ calculated from the PSD section. While the manual calculated fibril size of 51 nm±17 nm for the 40% stretched classic viscose is larger than for the 5% stretched viscose, the size of 40 $\mathrm{nm}^{+9\,\mathrm{nm}}_{-6\,\mathrm{nm}}$ determined from PSD is very similar. The MFA is 2.8° for the 5% stretched and 2.9° for the 40% stretched classic viscose.

The light spots, visible on the AFM phase image obtained from the 5% stretched classic viscose fiber, displayed in figure 4.36a are possibly contaminations from the manufacturing process.

4.2.5 Summary and comparison

Table 4.4 summarizes the characteristic values obtained from the discussed viscose fiber surfaces. Besides wrinkle size, fibril size, angle of wrinkles, and MFA also the surface roughness σ was calculated.

The surface wrinkles are probably induced by the spinneret in the manufacturing process and are for Bellini and Cellini fibers between 587 nm and 719 nm wide. Classical

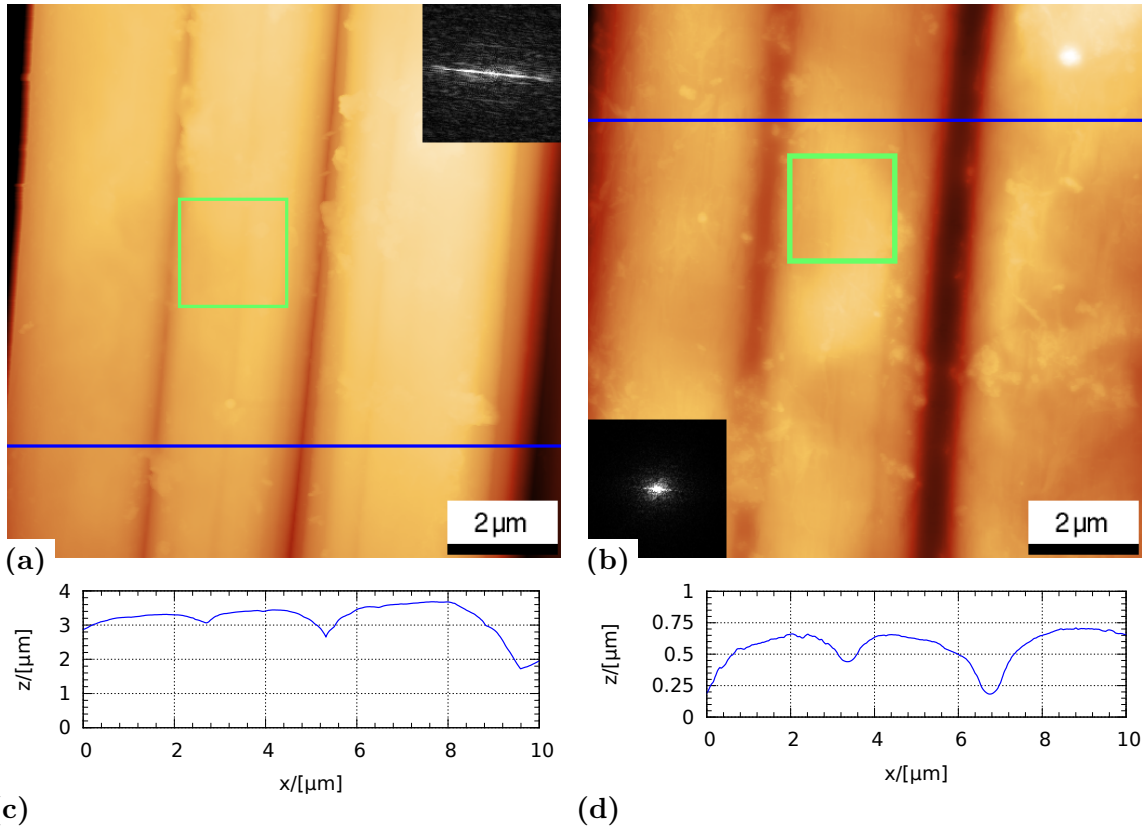

Figure 4.35: Classic viscose 10 μm×10 μm height images and line profiles. The blue lines indicate the positions of the profiles. (a) 5% stretched, z-scale: 3 μm. (b) 40% stretched, z-scale: 1 μm. Line profiles (c) to (a) and (d) to (b). The green squares in the height images mark the positions of figures 4.36a and 4.36b. The insets represent the 2D PSD of the AFM height image.

viscose has more pronounced surface wrinkles with a width of 3221 nm and 3716 nm for the 5% and the 40% stretched fibers, respectively.

The microfibril width was determined to be 30 nm for Bellini 1 and Bellini 4 fibers and 39 nm and 40 nm for 5% and 40% stretched classical viscose fibers.

For Bellini and Cellini fibers the surface roughness adopts low values between 71 nm and 80 nm and do not differ much from each other. For the 5% stretched classical viscose, a surface roughness of 513 nm is obtained, which is higher than the surface roughness of the 40% stretched fiber (129 nm).

The MFA is for both Bellini fibers near 0° and is about 3° for the classical viscose fibers. It was not possible to visualize fibrils on the Cellini fiber surface, due to the covering with CMC. The angle of the surface wrinkles to the fibers main axis is comparable to the MFA of the corresponding fiber, only the classical viscose fibers show lower values. This orientation of the wrinkles almost parallel to the fibers main axis might be a hint for an effect of the spinneret on the fiber surface.

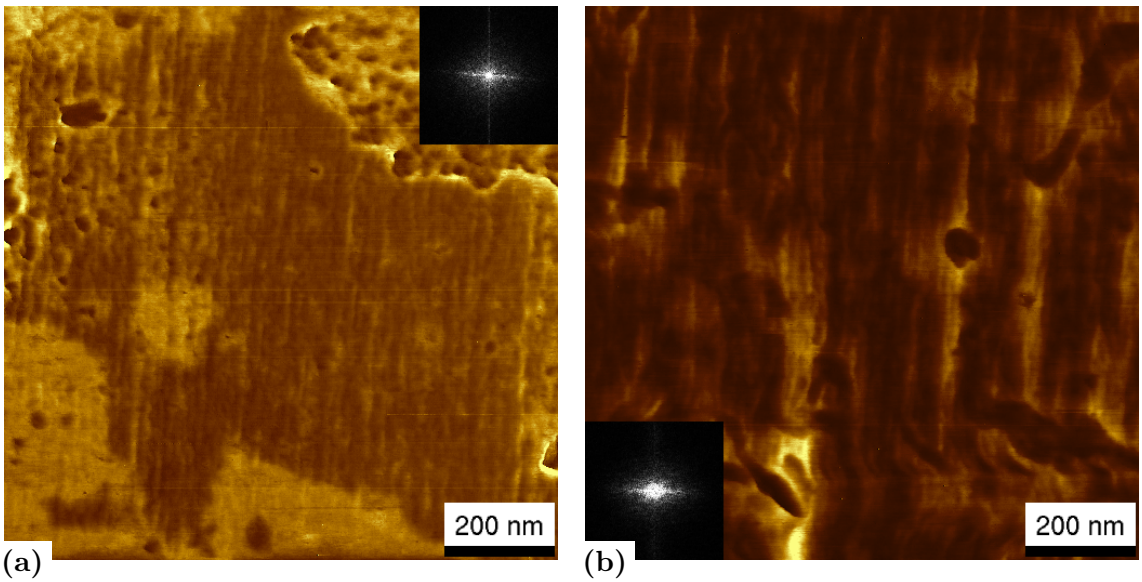

(a) (b)

Figure 4.36: Classic viscose 1 μm×1 μm phase images. (a) 5% stretched, z-scale: 15°. (b) 40% stretched, z-scale: 35°. The insets show the corresponding 2D PSD.

Table 4.4: Summary of characteristics obtained from viscose fiber surfaces. The values corresponding to classical viscose fibers were obtained from 10 μm×10 μm* AFM images, the others from 20 μm×20 μm AFM images. All sizes are obtained from PSD analysis.

Sample	wrinkle size	fibril size	σ	MFA	angle of wrinkles
	[nm]	[nm]	[nm]	[°]	[°]
Bellini 1	495^{+11}_{-11}	30^{+2}_{-2}	80	0.2	0.1
Bellini 4	719^{+45}_{-40}	30^{+3}_{-2}	76	0	0
Cellini 1	587^{+30}_{-26}	-	71	-	0.1
c. visc. 5%	3212^{+1992}_{-889}	39^{+4}_{-2}	513*	2.8	1.1
c. visc. 40%	3716^{+2564}_{-1078}	40^{+9}_{-6}	129*	2.9	2.1

5 Conclusions and Outlook

Conclusions

In this work, atomic force microscopy is presented as an unique technique to characterize surfaces of native cellulose fibers in wet and dry state and also regenerated viscose type cellulose fibers under ambient conditions. It was possible to visualize for each fiber type microfibrils with a width of 30 nm. In the wet state, height imaging revealed already single microfibrils on pulp fiber surfaces, while the fine structure of regenerated fiber surfaces was best determined by the application of AFM phase imaging.

First, industrial pulp fibers from Mondi showed a clear difference in surface structure when investigated in the wet and dried state. The surface of dried fibers was heavily wrinkled with a wrinkle size of about 500 nm, whereas never dried fibers offered a very smooth surface with a low amount of wrinkles, which were also less pronounced. The wet pulp fibers, measured in an aqueous environment, revealed single microfibrils in AFM topography images. HHCF and PSD analysis allowed a comprehensive surface characterization of temperature treated pulp fibers in wet state. The surface roughness seems not to be affected by temperature treatment, the lateral correlation length shows a slightly decreasing trend on spruce fiber surfaces and increases on pine fiber surfaces with temperature treatment. All spruce fibers were terminated by the S1 layer, which could be concluded by a high MFA in the range of 66° to 80°. The scanned areas on pine fiber surfaces revealed most of the time that the P layer is the exposed surface layer or a transition layer between P and S1 layer. Besides the microfibrils, also lignin precipitates were observable on the pulp fiber surfaces in AFM height images. The average sizes, the coverage, as well as the size distribution of the lignin precipitates could be determined. Scans on spruce fiber surfaces showed a decrease of lignin coverage with increasing temperature, whereas on pine fiber surfaces, first, a decrease and then an increase of lignin coverage with treatment temperature was observed. This could be interpreted as a dissolution of lignin at elevated temperatures and an reprecipitation of lignin with higher temperature.

Second, different stretched classical viscose fibers and fibers with a hollow and collapsed cross-section were investigated. The hollow and collapsed fibers, which are called by the industrial collaborator Kelheim Fibres GmbH Bellini 1, Bellini 4, and Cellini, offered a very flat and broad surface region and allowed to record AFM images with a scan size of $20\,\mu\text{m}\times20\,\mu\text{m}$. The classical viscose fiber samples allowed only recording of images with a scan size of $10\,\mu\text{m}\times10\,\mu\text{m}$ because of their curved surfaces. Cellini fibers are Bellini 4 fibers with the addition of CMC to increase their negative surface charge. Bellini and Cellini fiber surfaces showed surfaces wrinkles with a size of about 500 nm. On classical viscose fibers, wrinkles with a size of more than 3000 nm were

observed. The wrinkles were almost parallel to the fiber's main axis, only for classical viscose the angle of the wrinkles was about 1° to 2°. This might indicate an effect of the spinneret. From high-resolution phase images, fibrillar structures on the fiber surfaces with a size of 30 nm to 40 nm were visualized. Only on the Cellini fiber sample no fine structure could be resolved, due to the covering with CMC. The MFA is near by 0° for Bellini fibers and about 3° for classical viscose fibers. No significant difference in surface roughness is observable for Bellini and Cellini fibers. The surface roughness for classical viscose fibers is higher on the scanned region of the 5% stretched fiber. Bellini fibers seem to differ from each other only by the wrinkle size, which is higher for the Bellini 4 fiber. On Cellini fibers, the CMC can be visualized by AFM height images and its amount is calculated to be 15% of the scanned surface area.

Outlook

For further measurements it is planned to operate the fluid cell in the closed configuration to establish a closed environment where the humidity can be controlled. This setup would allow to obtain insight into the drying and rewetting process of pulp fiber surfaces by changing the relative humidity from 100% to 0% and recording AFM images for different humidity values. With that, hornification of the pulp fibers could be investigated in detail as this is a phenomenon that occurs during the drying process of pulp fibers and leads to irreversible changes in the fiber. A controlled humidity environment would allow to measure the very same area for all desired humidity values, which would provide comparable information of changes in fiber surface structure.

Further investigations of regenerated cellulose fibers may deal with the determination of CMC content on fiber surfaces with different amounts of CMC added. These AFM measurements will then be compared to infrared spectroscopy data, which can provide integral information on CMC content of a sheet formed from regenerated cellulose fibers. Also, the CMC-modified regenerated cellulose fibers will be investigated in water to study the influence of CMC on fiber swelling. To characterize electrical properties of regenerated cellulose fibers, Kelvin Probe Force Microscopy (KPFM) can be applied. Regenerated cellulose fibers would be a good choice for KPFM investigations, since they have not only a well defined surface morphology but also their composition is far more well defined than the composition of native cellulose fibers.

Acknowledgments

For helping me in the course of this work I want to thank

Ao.Univ.-Prof. Dipl.-Phys. Dr.rer.nat. Christian Teichert for his kind and excellent supervision, for teaching me about AFM and more, for giving me the opportunity to work in the SPM Group and to write this thesis and the correction of this work.

Dipl.-Ing. Dr.mont. Franz J. Schmied for teaching me AFM and cellulose fibers, for the excellent supervision, the kind and patient support and correction of this work.

Ao.Univ.-Prof. Mag. Dr.rer.nat. Robert Schennach , Graz University of Technology, and leader of the Christian Doppler Laboratory for "*Surface Chemical and Physical Fundamentals of Paper Strength*" for providing helpful information and support and the possibility to perform this work.

Dipl.-Ing. Johannes Leitner , Mondi, for sample preparation and helpful discussions.

Dipl.-Ing. Frederik Weber , Graz University of Technology, for helpful discussions and cooperation.

Dipl.-Ing. Dr.techn. Ulrich Hirn, Dipl.-Ing. Dr.techn. Rene Eckhart, Dipl.-Ing. Eduard Gilli, Dipl.-Ing. Wolfgang Fischer, Dipl.-Ing. Leo Arpa, Dr. Walter Rüf, Dr. Ingo Bernt and **Dr. Gerhard Zuckerstätter** for helpful discussions within the Christian Doppler Laboratory.

Dipl.-Ing. Dr.techn. Markus Kratzer for his help regarding AFM and analytical methods.

Dipl.-Ing. Stefan Lorbek for his help regarding AFM.

Ing. Heinz Pirker and **Peter Moharitsch** for their technical support.

Heide Kirchberger and **Magdalena Ottrin** for administrative support.

Dr.mont. Igor Beinik, Abdellatif Jerrar, Mario Lugger, Dipl.-Ing. Andreas Pavitschitz, Dipl.-Ing. Quan Shen, Astrid Wachauer and **Lin Wang** for giving me a nice and fun time and a good working atmosphere.

Christian Doppler Research Society for financial support.

My family

My friends and colleagues

List of Figures

List of Tables

Bibliography

[1] M.A. Hubbe and C. Bowden. Handmade paper: a review of its history, craft, and science. *BioResources*, 4(4):1736–1792, 2009.

[2] C.A.J. Putman, K.O. Van der Werf, B.G. De Grooth, N.F. Van Hulst, and J. Greve. Tapping mode atomic force microscopy in liquid. *Applied Physics Letters*, 64(18):2454–2456, 1994.

[3] N. Chhabra, J.K. Spelt, C.M. Yip, and M.T. Kortschot. An investigation of pulp fibre surfaces by atomic force microscopy. *Journal of Pulp and Paper Science*, 31(1):52–56, 2005.

[4] T. Sasaki, T. Okamoto, and G. Meshitsuka. Influence of deformability of kraft pulp fiber surface estimated by force curve measurements on atomic force microscope (AFM) contact mode imaging. *Journal of Wood Science*, 52(5):377–382, 2006.

[5] D. Ibarra, V. Köpcke, and M. Ek. Behavior of different monocomponent endoglucanases on the accessibility and reactivity of dissolving-grade pulps for viscose process. *Enzyme and Microbial Technology*, 47(7):355–362, 2010.

[6] Y. Yu, H. Kettunen, and K. Niskanen. Can viscose fibres reinforce paper? *Journal of Pulp and Paper Science*, 25(11):398–402, 1999.

[7] A. Torgnysdotter and L. Wågberg. Study of the joint strength between regenerated cellulose fibres and its influence on the sheet strength. *Nordic Pulp & Paper Research Journal*, 18(4):455–459, 2003.

[8] R.M. Rowell, R. Pettersen, J.S. Han, J.S. Rowell, and M.A. Tshabalala. Cell wall chemistry. In *Handbook of wood chemistry and wood composites*, pages 33–77. CRC Press, Boca Raton, 2005.

[9] E. Kontturi, T. Tammelin, and M. Österberg. Cellulose-model films and the fundamental approach. *Chemical Society Reviews*, 35(12):1287–1304, 2006.

[10] http://www.mondigroup.com/products/desktopdefault.aspx/tabid-160/, May 2011. Mondi.

[11] R.E. Booker and J. Sell. The nanostructure of the cell wall of softwoods and its functions in a living tree. *Holz als Roh- und Werkstoff*, 56(1):1–8, 1998.

[12] T. Zimmermann, E. Pöhler, and T. Geiger. Cellulose fibrils for polymer reinforcement. *Advanced Engineering Materials*, 6(9):754–761, 2004.

[13] M. Alava and K. Niskanen. The physics of paper. *Reports on Progress in Physics*, 69(3):669, 2006.

[14] M. Ek, G. Gellerstedt, and G. Henriksson. *Pulp and Paper Chemistry and Technology: Wood Chemistry and Wood Biotechnology*, volume 1. De Gruyter, Berlin, 2009.

[15] J.R. Barnett and V.A. Bonham. Cellulose microfibril angle in the cell wall of wood fibres. *Biological Reviews*, 79(02):461–472, 2004.

[16] P.J. Kleppe. Kraft pulping. *Tappi*, 53(1):35, 1970.

[17] M. Ek, G. Gellerstedt, and G. Henriksson. *Pulp and Paper Chemistry and Technology: Pulping Chemistry and Technology*, volume 2. De Gruyter, Berlin, 2009.

[18] D. Klemm, B. Heublein, H.P. Fink, and A. Bohn. Cellulose: faszinierendes Biopolymer und nachhaltiger Rohstoff. *Angewandte Chemie*, 117(22):3422–3458, 2005.

[19] A.C. O'Sullivan. Cellulose: the structure slowly unravels. *Cellulose*, 4(3):173–207, 1997.

[20] H. Harms. Fasertechnologie. Vorlesungsskriptum an der Montanuniversität Leoben, 2008.

[21] M.A. Rous, E. Ingolic, and K.C. Schuster. Visualisation of the fibrillar and pore morphology of cellulosic fibres applying transmission electron microscopy. *Cellulose*, 13(4):411–419, 2006.

[22] http://www.kelheim-fibres.com/newsletter/archiv/2010_02/faser.jpg, April 2011. Kelheim Fibres GmbH.

[23] E. Gilli, A.E. Horvath, A.T. Horvath, U. Hirn, and R. Schennach. Analysis of CMC attachment onto cellulosic fibers by infrared spectroscopy. *Cellulose*, 16(5):825–832, 2009.

[24] W. Nachtergaele. The benefits of cationic starches for the paper industry. *Starch-Stärke*, 41(1):27–31, 1989.

[25] G. Petzold, A. Nebel, H.M. Buchhammer, and K. Lunkwitz. Preparation and characterization of different polyelectrolyte complexes and their application as flocculants. *Colloid & Polymer Science*, 276(2):125–130, 1998.

[26] D.R. Biswal and R.P. Singh. Characterisation of carboxymethyl cellulose and polyacrylamide graft copolymer. *Carbohydrate Polymers*, 57(4):379–387, 2004.

[27] A. Baar, W.M. Kulicke, K. Szablikowski, and R. Kiesewetter. Nuclear magnetic resonance spectroscopic characterization of carboxymethylcellulose. *Macromolecular Chemistry and Physics*, 195(5):1483–1492, 1994.

[28] I. Elmadfa, D. Fritzsche, and E. Muskat. *E-Nummern & Zusatzstoffe*. Gräfe und Unzer, München, 2009.

[29] T. Takahashi, K. Tsunoda, H. Yajima, and T. Ishii. Dispersion and purification of single-wall carbon nanotubes using carboxymethylcellulose. *Japanese Journal of Applied Physics*, 43(no. 6 a):3636–3639, 2004.

[30] G. Binnig, C.F. Quate, and C. Gerber. Atomic force microscope. *Physical Review Letters*, 56(9):930–933, 1986.

[31] F.J. Giessibl. Atomic resolution on Si (111)-(7x7) by noncontact atomic force microscopy with a force sensor based on a quartz tuning fork. *Applied Physics Letters*, 76(11):1470–1472, 2000.

[32] Q. Zhong, D. Inniss, K. Kjoller, and V.B. Elings. Fractured polymer/silica fiber surface studied by tapping mode atomic force microscopy. *Surface Science Letters*, 290(1-2):L688–L692, 1993.

[33] J. Tamayo and R. García. Relationship between phase shift and energy dissipation in tapping-mode scanning force microscopy. *Applied Physics Letters*, 73(20):2926–2928, 1998.

[34] B. Anczykowski, J.P. Cleveland, D. Krüger, V. Elings, and H. Fuchs. Analysis of the interaction mechanisms in dynamic mode SFM by means of experimental data and computer simulation. *Applied Physics A: Materials Science & Processing*, 66(0):885–889, 1998.

[35] http://www.gwyddion.net, April 2011. Klapetek, P. and Necas, D.

[36] P. Hosemann. Characterization of cellulose fibers using Atomic-Force Microscopy. Master's thesis, Montanuniversität Leoben, 2004.

[37] F. J. Schmied. Characterization of cellulose type I and type II fibers using Atomic-Force Microscopy. Master's thesis, Montanuniversität Leoben, 2008.

[38] J.W. Cooley and J.W. Tukey. An algorithm for the machine calculation of complex Fourier series. *Math. Comput*, 19(90):297–301, 1965.

[39] M. Frigo and S.G. Johnson. The design and implementation of FFTW3. *Proceedings of the IEEE*, 93(2):216–231, 2005.

[40] C. Teichert. Self-organization of nanostructures in semiconductor heteroepitaxy. *Physics Reports*, 365(5-6):335–432, 2002.

[41] P. Klapetek, D. Necas, and C. Anderson. *Gwyddion user guide*, 2010.

[42] Y. Zhao, G.C. Wang, and T.M. Lu. *Characterization of amorphous and crystalline rough surface: principles and applications*. Academic Press, San Diego, 2001.

[43] K. Levenberg. A method for the solution of certain nonlinear problems in least squares. *Quart. Appl. Math*, 2(2):164–168, 1944.

[44] D.W. Marquardt. An algorithm for least-squares estimation of nonlinear parameters. *Journal of the society for Industrial and Applied Mathematics*, 11(2):431–441, 1963.

[45] F. J. Schmied. *Atomic Force Microscopy investigations of fiber-fiber bonds in paper*. PhD thesis, Montanuniversität Leoben, 2011.

[46] A.L. Zydney, P. Aimar, M. Meireles, J.M. Pimbley, and G. Belfort. Use of the log-normal probability density function to analyze membrane pore size distributions: functional forms and discrepancies. *Journal of Membrane Science*, 91(3):293–298, 1994.

[47] http://www.asylumresearch.com/Products/ClosedFluidCell/ClosedFluidCellDiagram.jpg, April 2011. Asylum Research.

[48] http://www.asylumresearch.com/ProbeStore/, April 2011. Asylum Research.

[49] http://probe.olympus-global.com/en/product/omcl_ac240ts_w2/, April 2011. OLYMPUS CORPORATION.